Trace Analyzer 2.0

December, 2017

Contents

I User's Guide **8**

1 Acknowledgement **9**

2 Typical Work Flow **10**

3 Modules of Trace Analyzer **12**
3.1 Material Editor 15
3.2 Layer Stackup Editor 17
3.2.1 Metal Layer Editor 18
3.2.2 Dielectric Layer Editor 20
3.3 Use of the Undercut Ratio 21
3.4 Remark on the z_offset Parameter 23
3.5 Trace Editor 24
3.6 Result Viewer 26

4 Benchmarks **27**
4.1 Single Microstrip 28
4.2 Coupled Microstrip 29
4.3 Single Stripline 30
4.4 Edge-Coupled Striplines 31
4.5 Ground Backed CPW with Dielectric Overlay 32
4.6 Broad-side Coupled Striplines 33
4.7 Coupled Buried Microstrip Traces with "under_cut" 34

5 Examples **36**
5.1 Broad-side Coupled Co-planar Lines 37
5.2 Shielded PCB Traces 38
5.3 Coupled Striplines in PCB 39
5.4 Coupled Microstrips in PCB 40

5.5 Coupled Striplines in Package . . . 41
5.6 Coupled Microstrips in Package . . . 42
5.7 Coupling between Differential Eight Traces in a Package Structure . . . 43
5.8 Differential Co-planar Design in a Thin-Film Structure . . . 44
5.9 Differential Microstrip Traces with Different Thickness . . . 45

6 File Formats 46
6.1 Layer Stackup File Format . . . 46
6.1.1 Example . . . 47
6.2 Trace Definition File Format . . . 50
6.2.1 Example . . . 50
6.3 Using RLGC Data in ADS . . . 51
6.3.1 Time-Domain Verification of RLGC Parameters Generated by TraceAnalyzer in ADS . . . 53

II Theoretical and Technical Notes 55

7 Multiconductor Transmission Line Theory 57
7.1 Frequency-Domain MTL Equations . . . 57
7.2 Propagation Constant and Characteristic Impedance Matrices . . . 59
7.3 Balanced Lossless Coupled Lines . . . 63
7.4 Slightly Unbalanced Lossless Coupled Lines . . . 67
7.5 Crosstalk Characterization . . . 70

8 Techniques of Finding the RLGC Parameters of MTL 71
8.1 Computing the L Matrix . . . 71
8.2 Computing the R Matrix . . . 72
8.3 Computing the G_d Matrix . . . 73

9 Calculation of the Capacitance Matrix in Trace Analyzer 74
9.1 Green's Function in Layered Media . . . 74
9.2 The spectral-domain Green's functions . . . 77
9.2.1 Generalized Reflection Coefficients . . . 77
9.2.2 Green's Functions for an Arbitrary Frequency . . . 79
9.2.3 The Static Green's Functions . . . 80
9.2.4 Complex Image Technique . . . 80
9.3 Method of Moment Formulation for Computing the C Matrix . . . 82

Bibliography **84**

List of Figures

2.1 Typical work flow of using Trace Analyzer. 10

3.1 Top-level GUI components of Trace Analyzer. 12
3.2 Menu items in Trace Analyzer. 13
3.3 Material Editor inside the Stackup tabbed-pane of the Main Panel. 15
3.4 Metal Layers Editor inside the Stackup tabbed-pane of the Main Panel. 18
3.5 Dielectric Layers Editor inside the Stackup tabbed-pane of the Main Panel. 20
3.6 Illustration of the usage of the under_cut ratio parameter. 21
3.7 Trace Editor of the Main Panel. 24
3.8 Result Viewer in the Main Panel. 26

4.1 Benchmark case of single microstrip. 28
4.2 Benchmark case of two coupled microstrips. 29
4.3 Benchmark case of single stripline. 30
4.4 Benchmark case of two coupled striplines. 31
4.5 Benchmark case of ground backed coplanar waveguide with dielectric overlay. . . . 32
4.6 Benchmark case of two broad-side coupled striplines. 33
4.7 Benchmark case of two coupled microstrips. 34

5.1 Broad-side coupled co-planar waveguide structure. 37
5.2 Impedance matrix of the broad-side coupled co-planar traces. 37
5.3 PCB traces with guard/shielding traces. 38
5.4 Impedance matrix of system including a single-ended signal and a pair of differential signal traces (with ground guards). 38
5.5 Coupled striplines in a PCB structure. 39
5.6 Impedance matrix of the coupled striplines in a PCB structure. 39
5.8 Impedance matrix of a pair of coupled microstrips in a PCB environment. 40
5.7 Coupled microstrips in a PCB layer. 40
5.9 Coupled striplines in a package structure. 41

5.10 Impedance matrix of the coupled striplines in a package structure. 41
5.12 Impedance matrix of a pair of coupled microstrips in a package environment. . . . 42
5.11 Coupled microstrips in a package layer. 42
5.13 Eight traces on two layers with additional coupling through a gap in plane. 43
5.14 Impedance matrix of eight coupled package traces. 43
5.15 Differentially coupled co-planar waveguide structure on a thin-film substrate. . . . 44
5.16 Impedance matrix of a differentially coupled co-planar waveguide pair. 44
5.17 Coupled microstrip traces with varying thickness. 45
5.18 Impedance matrix of coupled microstrip traces with different thickness. 45

6.1 Using RLGC data inside an ADS design. 52
6.2 Time-domain verification of using RLGC data inside ADS. 53

8.1 Scheme of computing skin resistance matrix. 72

9.1 Description of dielectric layers with infinite lateral extent (in x, y directions). Either the top or the bottom side may be terminated by a perfect electric conductor (PEC). 75
9.2 Traces in a multi-layered dielectric media. 82
9.3 Edges of a typical trace are divided into line segments. 82
9.4 One typical edge of a trace. 83

Preface

Transmission line has long been an important subject for microwave and RF engineers. With the advancement in digital technologies, especially when the clock and/or data rate reached multiple gigahertz (GHz), designers of printed circuit board (PCB) and package have to know the parameters like trace characteristic impedance and crosstalk, in order to maintain the signal integrity (SI). Over the years, the need for transmission line parameters of the traces rises steadily. Although some expensive PCB design and electromagnetic simulation software suites are capable of extracting transmission line parameters for given trace geometry and material information, electrical engineers still need an affordable and stand-alone trace analyzer software. Many web-sites respond to such need by providing on-line PCB calculators for one or two traces, mostly based on empirical formulas, which may give erroneous results, especially when the parameters are well outside of the validity ranges when the formulas were developed. Furthermore, real world engineering problems involve multiple traces in a layered dielectric media, and no empirical formulas can be found. In order to solve the general trace design problems, the tool has to be built based on solving Maxwell's equations. The topic of multiconductor transmission line (MTL) [1] was once a very active research area in the 1990's. Some of the mature methods are adopted in developing the current tool – Trace Analyzer.

This document is split into two parts. The first part is a user's guide for Trace Analyzer, which is essential for learning to use the tool. The second part provides under-the-hood theoretical details of the tool for the inquisitive users, which might also be useful to the advanced readers to develop their own MTL solvers.

Major features of Trace Analyzer include:

- Since Version 1.0
  - Integrated Material Editor.
  - Integrated Layer Stackup (Metal and Dielectric Layer) Editor.
  - Accommodating layered media with any number of dielectric/metal layers.
  - Length unit for the z-direction for layer stackup is unitZ, which is typically decided by the PCB manufacture. Unit for the x/y direction for traces is unitX. Trace Analyzer

allows unitZ and unitX to be different to relieve the user from conversion between the units.

- Designations of some metal layers to be connected to the ground (GND).
- Allowing any number of traces on any metal layers (except GND layers) with customized width and spacing rules.
- Calculations of RLGC matrices and the derived impedance matrix.
- Export RLGC parameters to W-element files compatible with HSPICE.
- Export RLGC parameters to model file compatible with ADS.
- File formats for storing material, layer stackup and trace design information.

- Added in Version 2.0

  - Activated the "under_cut" parameter as a property of a metal layer. This allows the cross sections of traces to take general trapezoidal shape.
  - Utilized the "z_offset" parameter as another property of a metal layer.
  - More accurate calculation method applied to stripline, and dual-stripline traces.
  - Calculation and report of crosstalk coefficients.
  - Calculation and report of modal conversion coefficient.

Part I

User's Guide

Chapter 1

Acknowledgement

- Trace Analyzer is written 100% in Java.
- The following Java numerical packages are instrumental building blocks in Trace Analyzer
  - Colt: a free Java toolkit at CERN for high performance computing. `URL:http://dsd.lbl.gov/~hoschek/colt/`
  - JAMA (JAva MAtrix package): contains common matrix routines. `http://math.nist.gov/javanumerics/jama/`
  - Jampack (JAva Matrix PACKage): matrix solver for complex matrices. `ftp://math.nist.gov/pub/Jampack/Jampack/AboutJampack.html`
- This document is prepared with $LaTeX$.

Chapter 2

Typical Work Flow

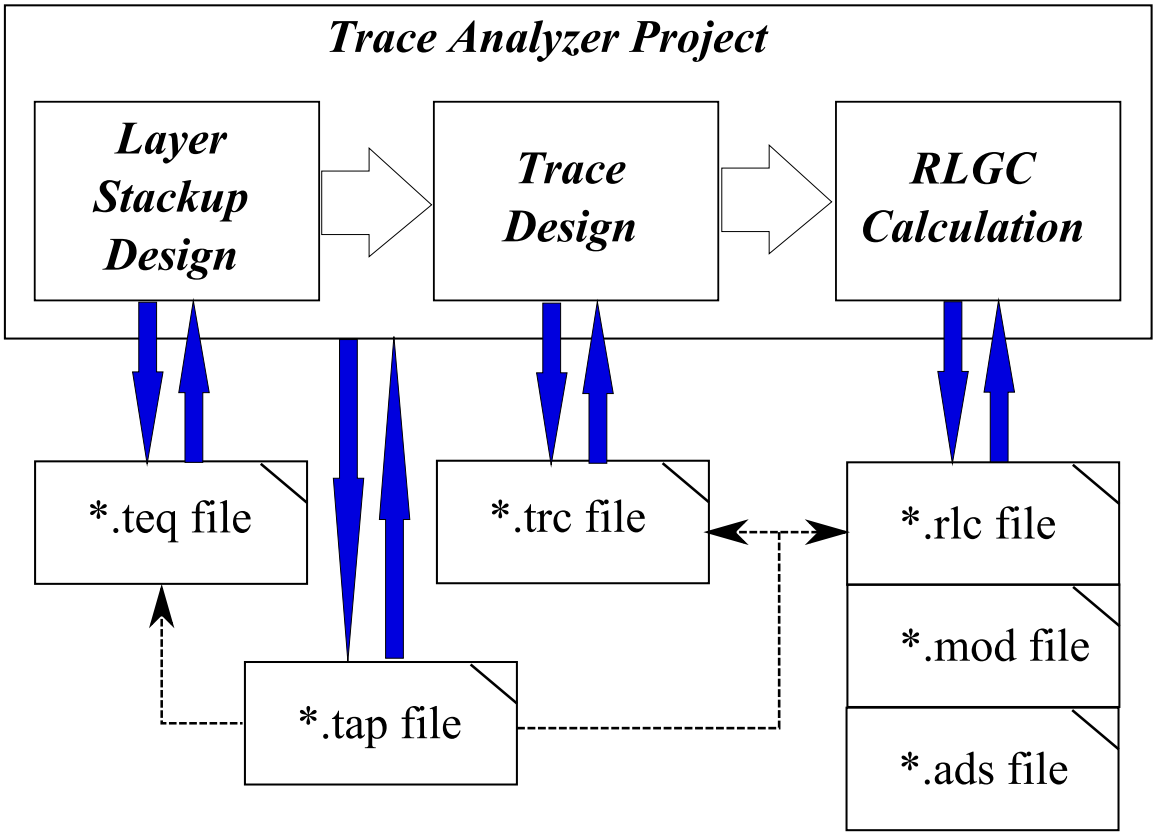

Figure 2.1: Typical work flow of using Trace Analyzer.

Information of the layer stackup and traces are stored into separate files, such that they are respectively reusable. Three types of files are essential in Trace Analyzer: (1) Technology file, a.k.a layer stackup file, with extension ".teq", (2) Trace file with extension ".trc", and (3) Trace Analyzer project file with extension ".tap".

Figure 2.1 is a diagram showing the typical work flow of Trace Analyzer. First, the user needs to establish a suitable layer stackup by defining the materials, dielectric and metal layers, which is saved in a ".teq" file. Next, traces are added by specifying the width and position coordinates, and saved in a ".trc" file. The collection of traces constitutes an MTL system, which can be solved for its R/L/G/C matrices. Results of the RLGC matrices can be stored in one of the standard file formats used by commercial simulation tools like HSPICE and ADS. The ".tap" file is the simplest, which has only two lines, binding the stackup and trace files, and optionally an RLGC file.

> The file names do not contain absolute directory names for maximum portability. As a consequence, **the layer stackup, traces, and RLGC files should always be kept in the same directory as the project file.** User may need to make copies when a stackup/trace file is shared by multiple projects.

Chapter 3

Modules of Trace Analyzer

Figure 3.1: Top-level GUI components of Trace Analyzer.

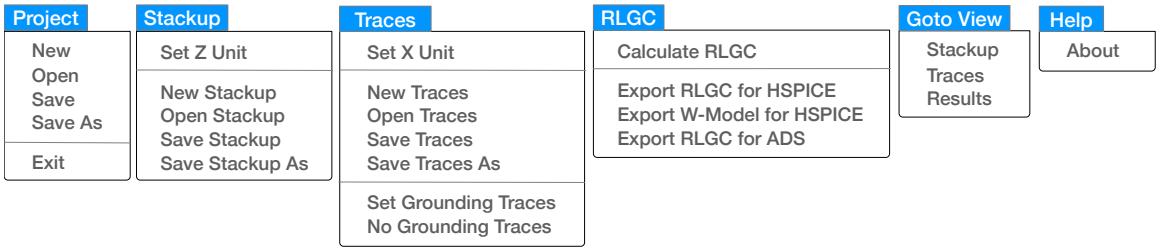

Figure 3.2: Menu items in Trace Analyzer.

Trace Analyzer, at the top-level, is composed of three major GUI parts: Menu bar, Main panel and Message area as shown in Figure 3.1. The menu items under Menu bar are:

- Project
  - New: start a new project. Any existing information about layer stackup, trace and RLGC will be flushed away;
  - Open: open an existing project file;
  - Save: update an existing project file with the latest modification;
  - Save As: save the current design information to a new project file;
  - Exit: exit the tool.
- Stackup
  - Set Z Unit: The Z direction is perpendicular to all metal/dielectric layers. User can choose a convenient unit, such as mm, mil, and um;
  - New Stackup: start a new layer stackup design. Any existing layer stackup information will be flushed away;
  - Open Stackup: open an existing layer stackup file;
  - Save Stackup: update an existing layer stackup file with the latest definitions;
  - Save Stackup As: save the current layer stackup information to a new layer stackup file.
- Traces
  - Set X Unit: The X direction is the one-dimensional coordinate system for trace position, width, spacing and etc.. User can choose the easiest unit suitable for the design;

  - New Traces: start a new composition of traces. Any existing trace definitions will be thrown away;
  - Open Traces: open trace design from an existing trace file;
  - Save Traces: update an existing trace file with the latest trace designs;
  - Save Traces As: save the current trace information to a new trace file;
  - Set Grounding Traces: allow user to specify some of the traces to be grounded. This is essential for analyzing the coplanar waveguide (CPW) structures;
  - No Grounding Traces: remove all the grounding designations from traces.

- RLGC

  - Calculate RLGC: start computations for R/L/G/C matrices;
  - Export RLGC for HSPICE: export RLGC file accepted by HSPICE;
  - Export W-Model for HSPICE: export RLGC model (another flavor) file accepted by HSPICE;
  - Export RLGC for ADS: export RLGC results to a file usable by ADS.

- Goto View: manually toggle between the following views. The selected view will occupy the Main Panel

  - Stackup;
  - Traces;
  - Results.

- Help

  - About: display the software and user license information.

The main panel shows one of the three views for manipulating stackup, traces, or displaying results, respectively. The user is presented with one of the views automatically according to typical flow. However, the user can jump to any view at any time with the "Goto View" menu. The tool may generate temporary data, status report and alerts, that are sent to the Message Area.

3.1 Material Editor

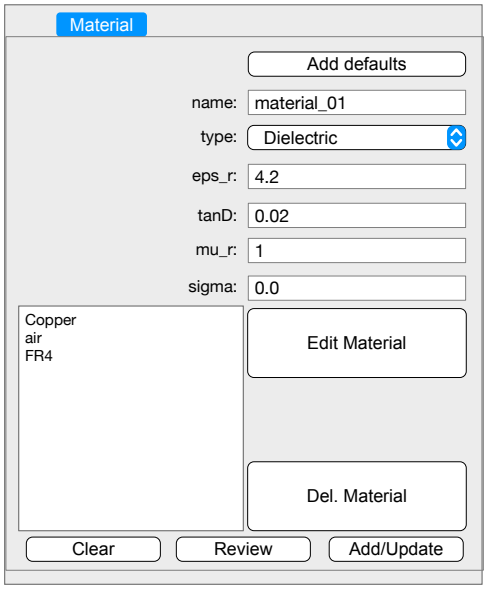

Figure 3.3: Material Editor inside the Stackup tabbed-pane of the Main Panel.

The Material Editor shown in Figure 3.3 provides support for composing materials used in the design. Typical actions required can be addressed through the appropriate sequences:

- Defining a new material
  - enter a new name in the "name:" text field;
  - choose "type:" to be either Dielectric or Metal;
  - enter a value for "eps_r" (required only for Dielectric type), the relative dielectric constant;
  - enter a value for "tanD" (ued only for Dielectric type), the dielectric loss tangent;
  - enter a value for "mu_r" (not used in the current version), the relative permeability;
  - enter a value for "sigma" (required only for Metal type), the conductivity;
  - click the "Add/Save" button. The newly added material should appear in the list.
- Modifying an existing material
  - select the material name from the list;

- click the "Edit Material" button. All the text fields will be updated with the selected material properties;
- make changes to any fields of interests;
- click the "Add/Save" button.

3.2 Layer Stackup Editor

Layer stackup is a technical jargon used by the designers of printed circuit boards (PCBs) or packages. It specifies how the dielectric layers are stacked, and how the metal layers are sandwiched between the dielectric layers. The following essential assumptions are very important to the user:

- A stackup is always implicitly terminated by one air (or vacuum) layer of semi-infinite thickness on the top-most dielectric layer, and one air layer of semi-infinite thickness below the bottom-most dielectric layer.
- Dielectric layers are introduced first in top-down order.
- Conceptually, metal layers are anchored at the interior boundaries between pairs of adjacent dielectric layers.
  - No metal layer can be defined on either the top-air or bottom-air boundary.
- When a stackup is created and managed by Trace Analyzer, the convention is: **There are always (N+1) dielectric layer for N metal layers.** However, it is possible, but not advisable, for user to manually create a stackup file which brakes this convention.
  - User can define the number of metal layers first to be N (insides the Metal Layer Editor). Then, the number of dielectric layers will be automatically fixed to (N+1);
  - User can also define the number of dielectric layers first to be Nd (insides the Dielectric Layer Editor). Then, the number of metal layers will be automatically set to (Nd-1);
- At each dielectric layer boundary, when the "is plane" flag turned off, a metal layer normally is immersed into either of the abutting dielectric layer, which can take either "below" or "above" position with respect to the boundary. A special position of the metal layer is assigned by turning on the "is plane" flag to indicate that the entire metal layer is inserted.
- Metal/dielectric layers are indexed from 1 at the top and increasing toward the bottom.

The overall layer stackup editing capabilities are realized by the Metal Layer Editor and the Dielectric Layer Editor.

3.2.1 Metal Layer Editor

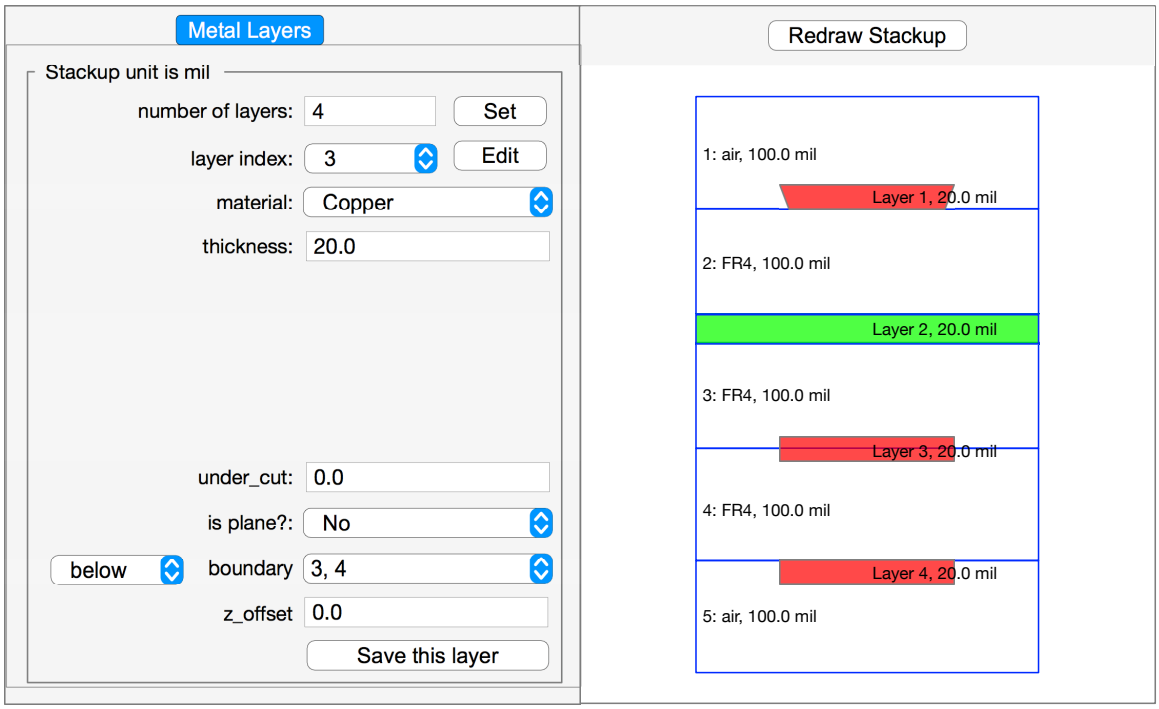

Figure 3.4: Metal Layers Editor inside the Stackup tabbed-pane of the Main Panel.

The Metal Layer Editor shown in Figure 3.4 facilitates the following common tasks:

- Set number of metal layers
  - simply fill in the text field “number of layers:” with the desired number, then click the "Set" button.
- Set metal layer attributes
  - choose the “layer index” from drop-down list;
  - optionally, click button “Edit” to load the stored attributes associated with this layer;
  - choose a “material:” name based on available metal materials;
  - set “thickness” using the current Z-unit. User can double check the Z-unit by invoking menu “Stackup::Set Z Unit”;

- the “undercut:” specifies the undercut ratio;
- set the “is plane?” flag;
- set the “above/below” choice;
- the “z_offset” is the additional z-coordinate offset with respect to the boundary;
- click the “Save this layer” button to update.

3.2.2 Dielectric Layer Editor

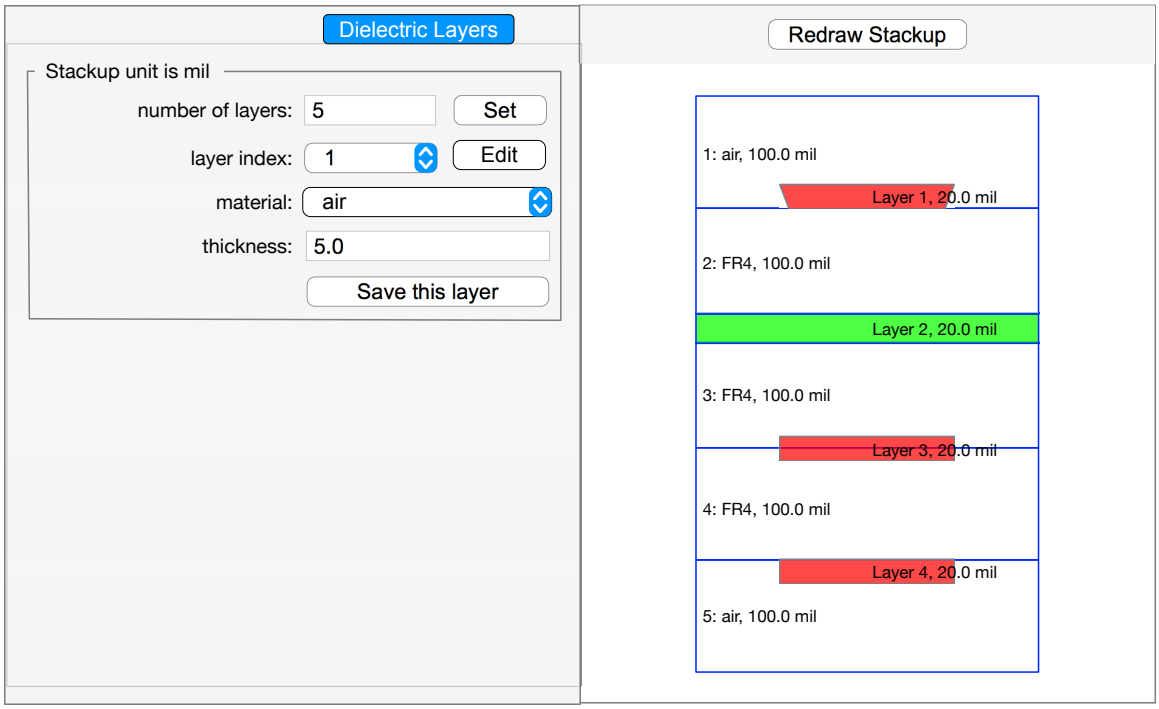

Figure 3.5: Dielectric Layers Editor inside the Stackup tabbed-pane of the Main Panel.

The Dielectric Layer Editor shown in Figure 3.5 facilitates the following common tasks:

- Set number of dielectric layers
  - simply fill in the text field “number of layers:” with the desired number, then click the "Set" button.
- Set dielectric layer attributes
  - choose the “layer index” from drop-down list;
  - optionally, click button “Edit” to load the stored attributes associated with this layer;
  - choose a “material:” name based on available dielectric materials;
  - set “thickness” using the current Z-unit. User can double check the Z-unit by invoking menu “Stackup::Set Z Unit”;
  - click the “Save this layer” button to update.

3.3 Use of the Undercut Ratio

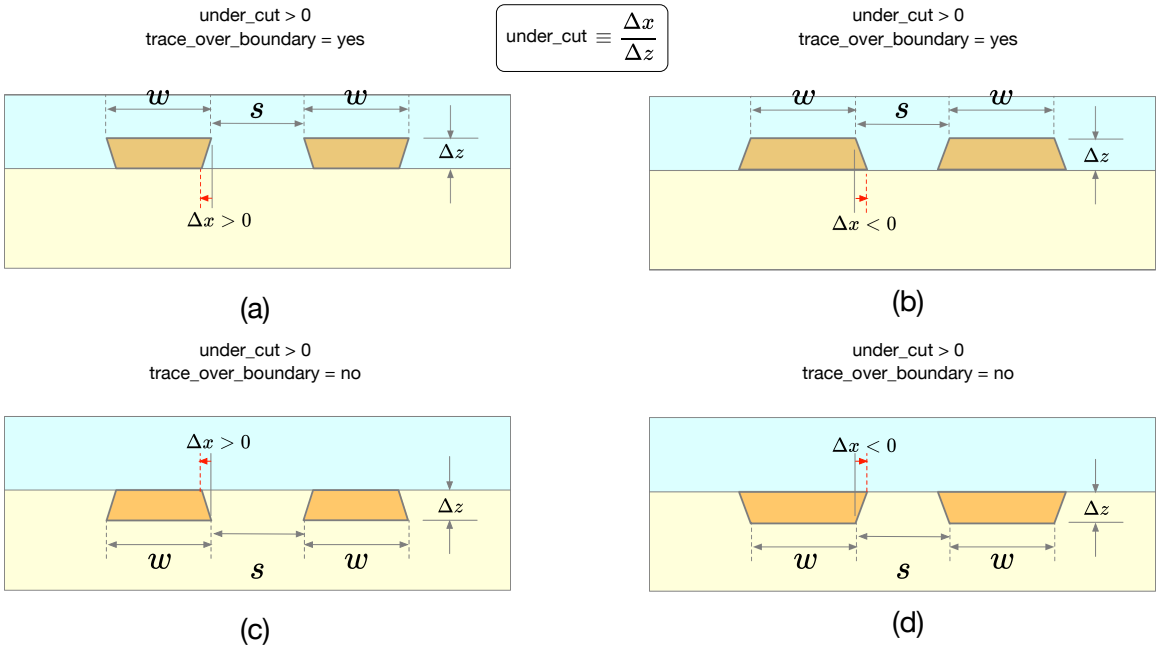

Figure 3.6: Illustration of the usage of the under_cut ratio parameter.

A property of a metal layer called "under_cut," has been introduced since Version 1.0 of this software. But, it is only activated in Trace Analyzer 2.0. "under_cut" is used to characterize the uneven etching effect associated with the real-world PCB manufacturing process. Illustrated by Figure 3.6, the "under_cut" parameter is defined with the following considerations:

- The nominal width of a metal trace is the width of the surface that is not on the anchoring dielectric boundary
  - When the trace is above the boundary, trace width refers to the width of the top surface, as shown in 3.6(a), and (b)
  - When the trace is below the boundary, trace width refers to the width of the bottom surface, as shown in 3.6(c), and (d)
  - Positive value of under_cut means that the surface on the boundary is narrower, as with 3.6(a) and (c)
  - Negative value of under_cut means that the surface boundary is wider, as with 3.6(b) and (d)

  - The parameter under_cut is essentially the tangent of the angle between the trace side-wall with respect to the vertical line

- If Δz refers to the trace thickness (assumed to be always a positive number), and Δx refers to the horizontal displacement at each side, then

$$\text{under\_cut} \equiv \frac{\Delta x}{\Delta z}$$

This parameter allows the use of trapezoidal shapes to more truthfully describe the actual trace geometry.

3.4 Remark on the z_offset Parameter

Another property associated with a metal layer is "z_offset," which has existed since Version 1.0, too. But, it has not been utilized until now. After the position of a metal layer is defined by

1. anchoring boundary between two dielectric layers
2. above/below boundary property

a additional vertical movement is assessed, specified by the value of "z_offset". Positive z_offset moves a trace upward, while negative z_offset moves a trace downward. The use of this parameter provide additional flexibility for the tool.

> Note that this parameter has no effect on either a metal plane layer, or a dielectric layer.

3.5 Trace Editor

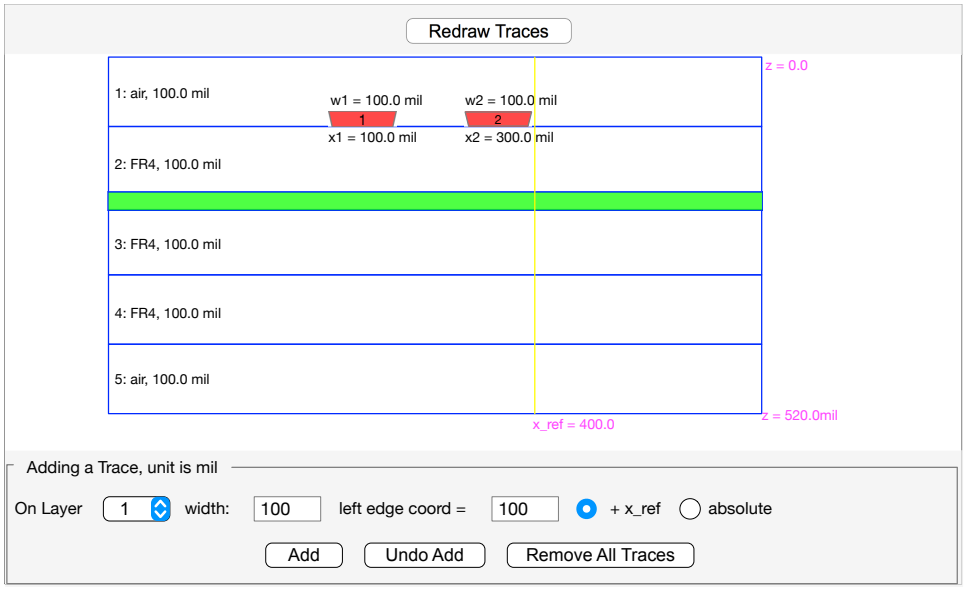

Figure 3.7: Trace Editor of the Main Panel.

The Trace Editor shown in Figure 3.7 is designed to minimize the user's effort in specifying the trace geometry information. There are a few conventions and operations that the user should get familiar with:

- Each trace is fully specified by
  - the metal layer index;
  - the X-coordinate of the left edge, which is labeled immediately below the trace;
  - trace width, which is labeled immediately above the trace.
- The text field after "width" specifies the next trace width.
- The text field after "left edge coordinate:" is assigned to the Xin variable.
- The tool always keeps an X-REFERENCE value (which is 0 initially);
  - X-REFERENCE holds the coordinate of the right edge of the last added trace.
- User can toggle between two coordinate modes by clicking the appropriate radio button:

  - in the "relative to the right edge of last trace" mode, the new trace left edge coordinate is X = Xin + X-REFERENCE;
  - in the "absolute" mode, the new trace left edge coordinate is X = Xin.

- Click on the "Add" button will add a new trace.
- Click on the "Remove Last Trace" will remove the last added trace.
- To start a new design, use menu item "Traces::New Trace".

3.6 Result Viewer

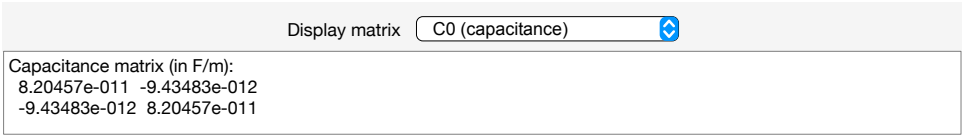

Figure 3.8: Result Viewer in the Main Panel.

Upon the completion of the RLGC calculation, the results can be immediately displayed for visual inspection. As shown Figure 3.8, a drop-down list can be used to choose reporting of one of the following parameters:

- Lo: inductance matrix;
- Co: capacitance matrix;
- Ro: DC resistance matrix;
- Rs: skin-effect resistance matrix;
- Gd: AC conductance matrix;
- per-unit-length delay;
- phase velocity;
- characteristic impedance;
- crosstal coefficients;
- modal conversion coefficient.

Chapter 4

Benchmarks

To ensure the accuracy of the tool, some benchmark cases have been developed. In most applications, the L and C matrices are the most important parameters. To minimize complications, the characteristic impedances under lossless condition (or equivalently letting frequency to approach infinity while ignoring Gd), by setting R's and G's to zeros, are used for comparison. At least one other established MTL tools are used to solve the same problem with impedance number tabulated. In those cases, the relative differences of impedance values generated by Trace Analyzer are less than 3%.

4.1 Single Microstrip

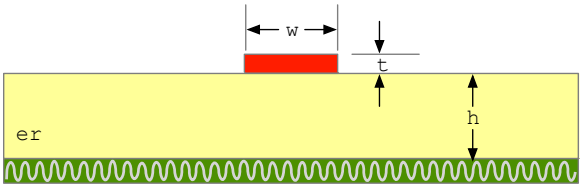

Figure 4.1: Benchmark case of single microstrip.

The parameters for the microstrip are given below:

- w = 10 mil
- t = 2.8 mil
- h = 8 mil
- er = 5.23

Characteristic impedance values from measurement [2], and LINPAR [3], a method of moment (MOM) tool, are listed below:

Method	Z0 (ohm)
Measurement	53
LINPAR	53.82
Trace Analyzer	53.57

The files can be found in /benchmarks/microstrip1.

4.2 Coupled Microstrip

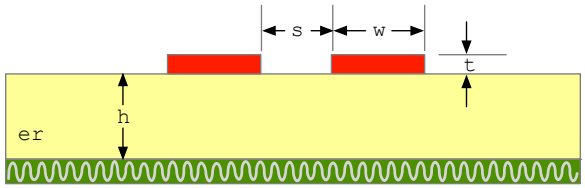

Figure 4.2: Benchmark case of two coupled microstrips.

The parameters for the two microstrips are given below:

- w = 10 mil
- s = 5 mil
- t = 2.8 mil
- h = 8 mil
- er = 5.23

Characteristic impedance values from measurement, and LINPAR, a method of moment (MOM) tool, are listed below:

Method	Zodd (ohm)	Zeven (ohm)
LINPAR	38.47	65.67
Trace Analyzer	38.40	65.33

The files can be found in /benchmarks/microstrip2.

4.3 Single Stripline

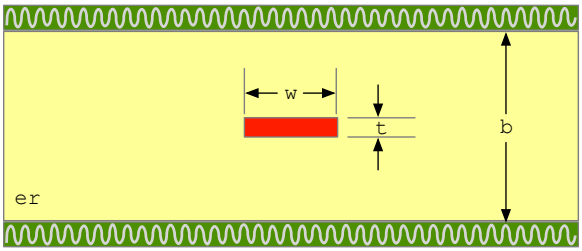

Figure 4.3: Benchmark case of single stripline.

The parameters for the stripline are given below:

- w = 12.5 um
- b = 25.4 um
- t = 1.4 um
- er = 3.25

The characteristic impedance values computed by FlexPDE [4] (pp. 242-243), a finite element (FEM) tool, and LINPAR, a method of moment (MOM) tool, are listed below:

Method	Z0 (ohm)
FlexPDE	50
LINPAR	49.59
Trace Analyzer	50.02

The files can be found in /benchmarks/stripline1.

4.4 Edge-Coupled Striplines

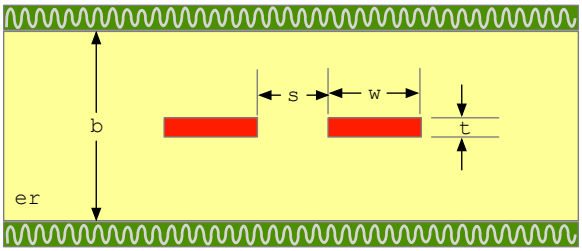

Figure 4.4: Benchmark case of two coupled striplines.

The parameters for the coupled striplines are given below:

- w = 11.7 um
- s = 6.4 um
- b = 25.4 um
- t = 1.4 um
- er = 3.25

Characteristic impedance values computed by FlexPDE [4] (pp. 246-248), a finite element (FEM) tool, and LINPAR, a method of moment (MOM) tool, are listed below:

Method	Zodd (ohm)	Zeven (ohm)
FlexPDE	41.05	60.56
LINPAR	40.82	59.75
Trace Analyzer	41.02	60.37

The files can be found in /benchmarks/stripline2.

4.5 Ground Backed CPW with Dielectric Overlay

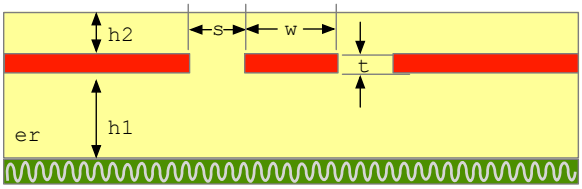

Figure 4.5: Benchmark case of ground backed coplanar waveguide with dielectric overlay.

The above structure has a dielectric overlay which doesn't fit into the standard template of many solvers, but it is easily handled by Trace Analyzer. The parameters for the stripline are given below:

- w = {30, 60} mil
- s = 15 mil
- t = 0 mil (2 mil is used in Trace Analyzer)
- h1 = 42 mil
- h2 = 20 mil
- er = 4.4

Characteristic impedance value computed by QuickField [4] (pp. 250-251), a finite element (FEM) tool is listed below:

Method	Z0 (ohm), w = 30 mil	Z0 (ohm), w = 60 mil
QuickField	49.26	40.11
Trace Analyzer	50.43	38.97

The files can be found in /benchmarks/gcpw.

4.6 Broad-side Coupled Striplines

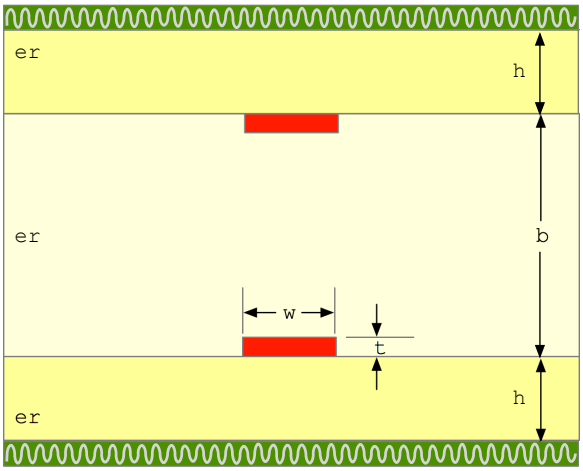

Figure 4.6: Benchmark case of two broad-side coupled striplines.

A pair of broad-side coupled stripline traces are shown in Figure 4.6 with parameters of:

- w = 125 um
- t = 17 um
- h = 300 um
- b = 1000 um
- er = 4.8

Per-unit length capacitance, inductance parameters are calculated using Trace Analyzer 2.0, compared with results from ANSYS Q2D Extractor (at 5 GHz):

Method	C11(F/m)	|C12| (F/m)	L11 (H/m)	L12 (H/m)	Zcomm	Zdiff
Q2D	1.01E-10	7.16E-12	5.37E-7	3.74E-8	39.03	135.7
Trace Analyzer	9.92E-11	7.12E-12	5.41E-7	3.88E-8	39.67	137.4

The files can be found in /benchmarks/broadside.

4.7 Coupled Buried Microstrip Traces with "under_cut"

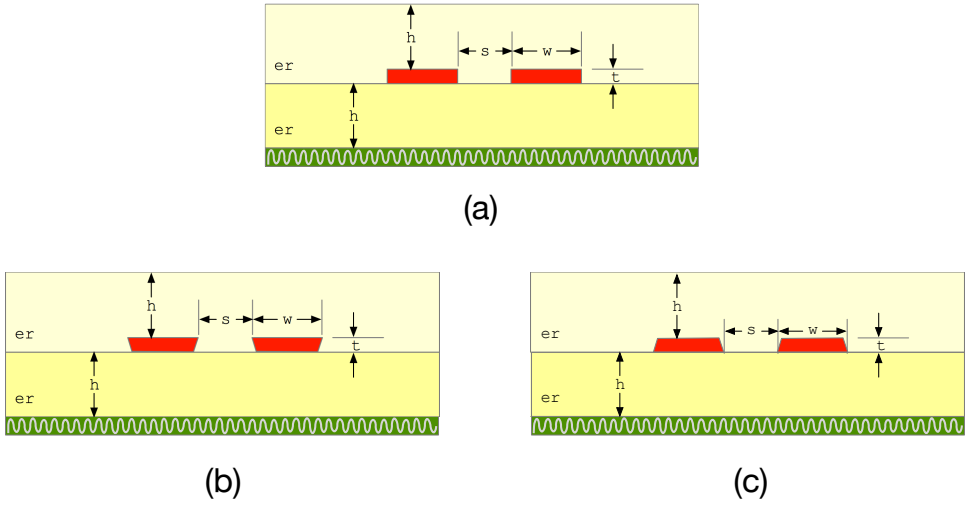

Figure 4.7: Benchmark case of two coupled microstrips.

Two buried microstrip traces with the primary parameters defined below:

- w = 100 um
- s = 100 um
- t = 20 um
- h = 100 um
- er = 4.2

The reference case is shown in Figure 4.7(a). And a under_cut ratio of +/-0.6 is applied in 4.7(b) and (c). The subtle difference made by the under_cut is manifested by the results calculated by Trace Analyzer 2.0, compared with simulation data from ANSYS Q2D Extractor (at 5 GHz).

For the reference case of Figure 4.7(a):

Method	C11 (F/m)	|C12| (F/m)	L11 (H/m)	L12 (H/m)	Zcomm	Zdiff
Q2D	1.247E-10	3.071E-11	3.754E-7	8.593E-8	35.02	86.30
Trace Analyzer	1.218E-10	3.175E-11	3.756E-7	8.567E-8	35.79	86.91

For the case of Figure 4.7(b):

Method	C11 (F/m)	|C12| (F/m)	L11 (H/m)	L12 (H/m)	Zcomm	Zdiff
Q2D	1.179E-10	2.765E-11	3.931E-7	8.607E-8	36.44	91.87
Trace Analyzer	1.162E-10	2.858E-11	3.929E-7	8.584E-8	36.95	92.10

For the case of Figure 4.7(c):

Method	C11 (F/m)	|C12| (F/m)	L11 (H/m)	L12 (H/m)	Zcomm	Zdiff
Q2D	1.200E-10	2.772E-11	3.884E-7	8.323E-8	35.71	90.84
Trace Analyzer	1.164E-10	2.970E-11	3.882E-7	8.300E-8	36.86	91.41

The files can be found in /benchmarks/uc_ustrip2.

Chapter 5

Examples

The benchmark results in the previous chapter illustrated the accuracy this tool. More practical examples are shown in this chapter to analyze traces used in various realistic substrate environment such as PCB, package, and thin-film designs. With the popularity of differential signaling in higher speed operations, more than half of the examples try to target a differential impedance about 100 ohm. These project files reside in the example sub-directory of the program distribution.

5.1 Broad-side Coupled Co-planar Lines

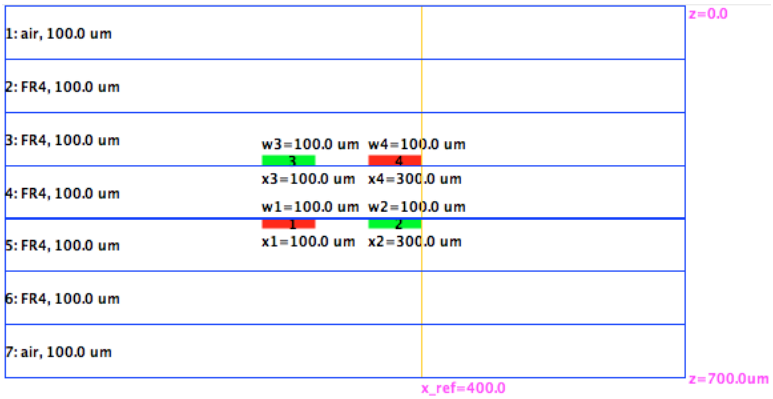

Figure 5.1: Broad-side coupled co-planar waveguide structure.

Four PCB traces are routed on two adjacent metal layers as shown in Figure 5.1. The dielectric constant is 4.2. Two of the traces are grounded, results in a co-planar transmission-line in each layer. Due to the proximity of the traces, the two sets of the co-planar lines are strongly coupled. The resultant impedance matrix is shown in Figure 5.2. This project file is under /examples/bc_cpw.

```
Characteristic impedance in (Ohm), ignoring losses:
  5.97615e+001  6.99677e+000
  6.99677e+000  5.97569e+001
Note: when N=2 and nearly symmetric
   Zcomm ~ (Z11+Z12)/2; Zdiff ~ 2*(Z11-Z12)
```

Figure 5.2: Impedance matrix of the broad-side coupled co-planar traces.

5.2 Shielded PCB Traces

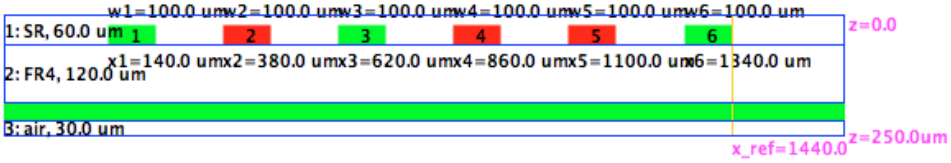

Figure 5.3: PCB traces with guard/shielding traces.

Six PCB traces are laid out on a microstrip layer as shown in Figure 5.3. Three of the lines are tied to ground, resulting in a single-ended trace and a pair of differential signal traces. The coupling effect between the single-ended and differential traces are reflected in the final impedance matrix in Figure 5.4. This project file is under /examples/pcb_shield.

Characteristic impedance in (Ohm), ignoring losses:

5.70099e+001	9.78143e-001	5.49623e-001
9.78143e-001	5.90887e+001	1.11431e+001
5.49623e-001	1.11431e+001	5.90997e+001

Figure 5.4: Impedance matrix of system including a single-ended signal and a pair of differential signal traces (with ground guards).

5.3 Coupled Striplines in PCB

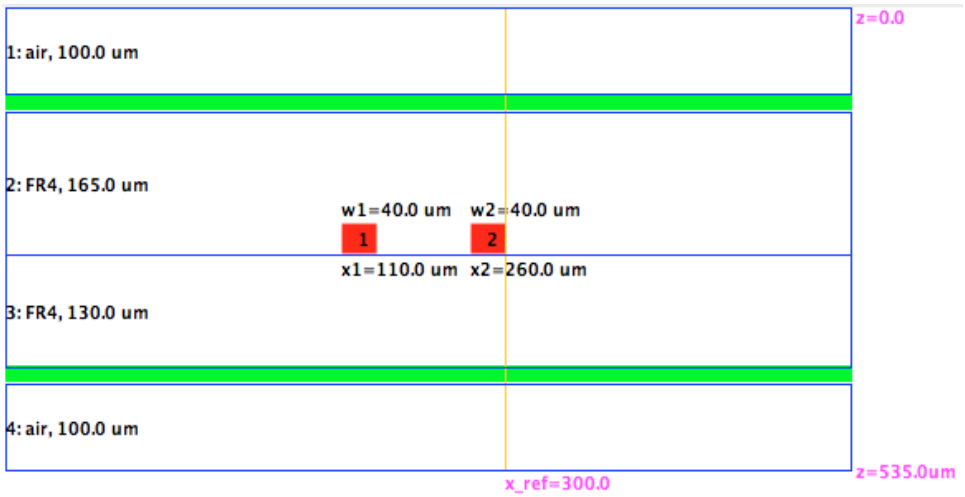

Figure 5.5: Coupled striplines in a PCB structure.

A pair of traces are routed in a PCB stripline layer as shown in Figure 5.5. The trace widths are 40 um, with spacing of 110 um. The resultant impedance matrix is shown in Figure 5.6. This project file is under /examples/pcb_stripline2.

```
Characteristic impedance in (Ohm), ignoring losses:
  Even mode: 7.43532e+001, Common mode: 3.71766e+001
  Odd mode: 5.01543e+001, Differential mode: 1.00309e+002
```

Figure 5.6: Impedance matrix of the coupled striplines in a PCB structure.

```
Characteristic impedance in (Ohm), ignoring losses:
  Even mode: 7.57138e+001, Common mode: 3.78569e+001
  Odd mode: 4.96589e+001, Differential mode: 9.93178e+001
```

Figure 5.8: Impedance matrix of a pair of coupled microstrips in a PCB environment.

5.4 Coupled Microstrips in PCB

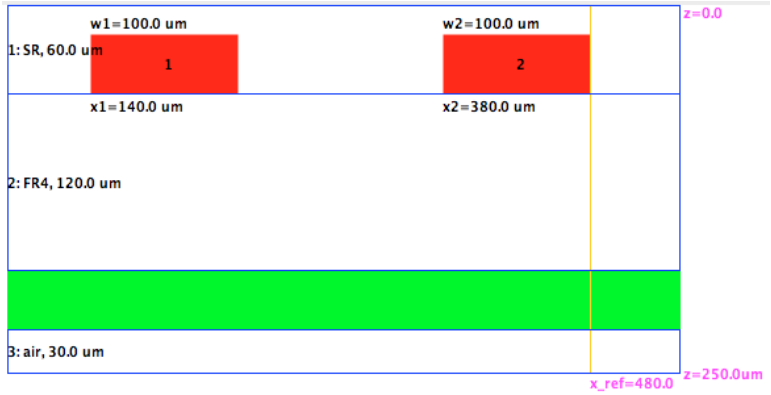

Figure 5.7: Coupled microstrips in a PCB layer.

Two coupled microstrips are laid in a PCB structure as shown in Figure 5.7. The trace widths are 100 um, with spacing of 140 um. The calculated impedance matrix is shown in Figure 5.8. This project file is under /examples/pcb_ustrip2.

5.5 Coupled Striplines in Package

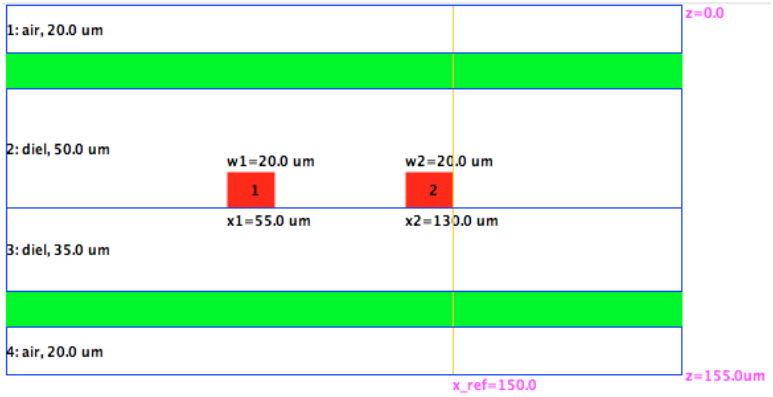

Figure 5.9: Coupled striplines in a package structure.

A pair of traces are routed in a package stripline layer as shown in Figure 5.9. The trace widths are 20 um, with spacing of 55 um. The resultant impedance matrix is shown in Figure 5.10. This project file is under /examples/pkg_stripline2.

```
Characteristic impedance in (Ohm), ignoring losses:
  Even mode: 5.82202e+001, Common mode: 2.91101e+001
  Odd mode: 4.97850e+001, Differential mode: 9.95700e+001
```

Figure 5.10: Impedance matrix of the coupled striplines in a package structure.

```
Characteristic impedance in (Ohm), ignoring losses:
  Even mode: 1.14124e+002, Common mode: 5.70619e+001
  Odd mode: 5.02291e+001, Differential mode: 1.00458e+002
```

Figure 5.12: Impedance matrix of a pair of coupled microstrips in a package environment.

5.6 Coupled Microstrips in Package

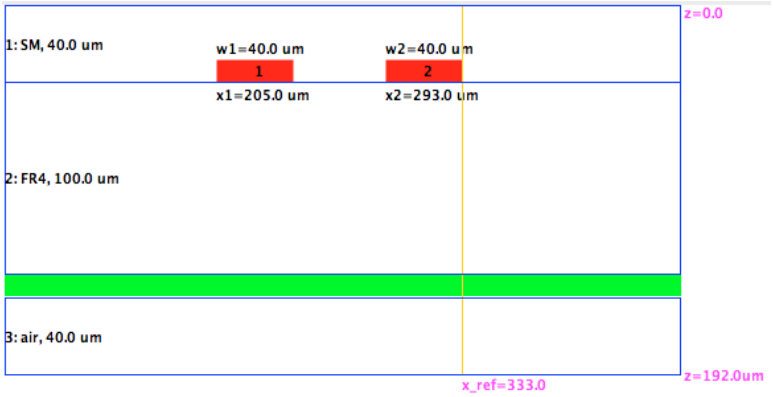

Figure 5.11: Coupled microstrips in a package layer.

Two coupled microstrips are laid in a PCB structure as shown in Figure 5.11. The trace widths are 100 um, with spacing of 140 um. The calculated impedance matrix is shown in Figure 5.12. This project file is under /examples/pkg_ustrip2.

5.7 Coupling between Differential Eight Traces in a Package Structure

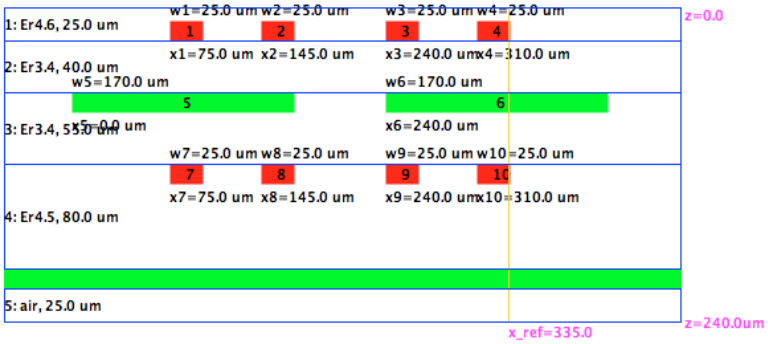

Figure 5.13: Eight traces on two layers with additional coupling through a gap in plane.

As shown in Figure 5.13, eight traces are laid in a package environment, with four on Layer 1 and four on Layer 3. Layer 2 is primarily a ground plane, but with a slot opening of size 70 um. The presence of the gap causes couplings between all traces. The calculated impedance matrix is shown in Figure 5.14. This project file is under /examples/pkg_xtk.

Characteristic impedance in (Ohm), ignoring losses:

6.72867e+001	1.68400e+001	2.78062e+000	3.48300e-003	-1.65522e-001	-1.10466e-001	-1.42732e-001	-2.51296e-001
1.68400e+001	6.88927e+001	1.11806e+001	2.78062e+000	-1.29204e-001	4.33877e-001	3.72118e-001	-1.65563e-001
2.78062e+000	1.11806e+001	6.88927e+001	1.68400e+001	-1.65563e-001	3.72118e-001	4.33877e-001	-1.29204e-001
3.48300e-003	2.78062e+000	1.68400e+001	6.72867e+001	-2.51296e-001	-1.42732e-001	-1.10466e-001	-1.65522e-001
-1.65522e-001	-1.29204e-001	-1.65563e-001	-2.51296e-001	5.60069e+001	1.13965e+001	2.62791e+000	1.67798e+000
-1.10466e-001	4.33877e-001	3.72118e-001	-1.42732e-001	1.13965e+001	5.69381e+001	7.30992e+000	2.62791e+000
-1.42732e-001	3.72118e-001	4.33877e-001	-1.10466e-001	2.62791e+000	7.30992e+000	5.69381e+001	1.13965e+001
-2.51296e-001	-1.65563e-001	-1.29204e-001	-1.65522e-001	1.67798e+000	2.62791e+000	1.13965e+001	5.60069e+001

Figure 5.14: Impedance matrix of eight coupled package traces.

5.8 Differential Co-planar Design in a Thin-Film Structure

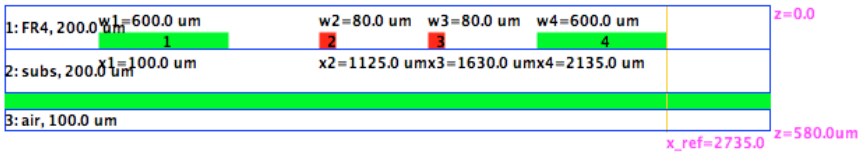

Figure 5.15: Differentially coupled co-planar waveguide structure on a thin-film substrate.

On a thin-film substrate, a pair of differentially coupled co-planar lines are designed as shown in Figure 5.15. The width is 80 um, and spacing of 425 um. The distance between the outer edges of the differential pair and the ground planes are also 425 um. The calculated impedance matrix is shown in Figure 5.16. This project file is under /examples/tf_dcpw.

```
Characteristic impedance in (Ohm), ignoring losses:
  Even mode: 5.18674e+001, Common mode: 2.59337e+001
  Odd mode: 4.37620e+001, Differential mode: 8.75240e+001
```

Figure 5.16: Impedance matrix of a differentially coupled co-planar waveguide pair.

5.9 Differential Microstrip Traces with Different Thickness

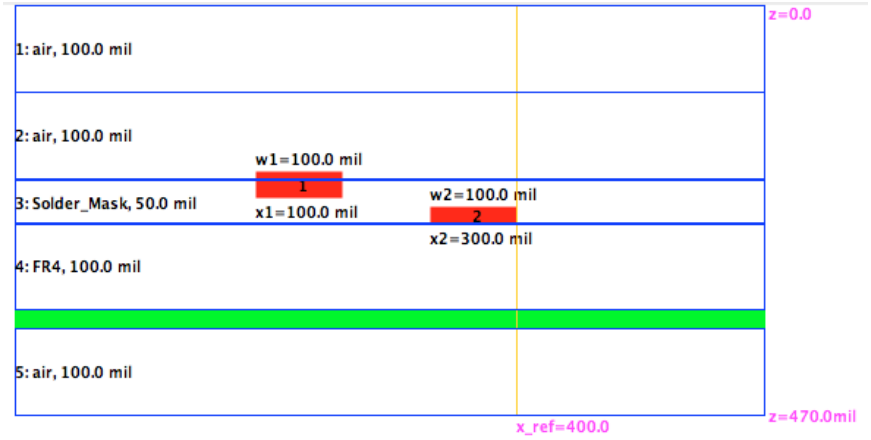

Figure 5.17: Coupled microstrip traces with varying thickness.

Two coupled microstrip traces with different thickness, not horizontally aligned, are shown in Figure 5.17. The width and spacing are both 100 mils. The thickness for the two traces are 30 mils and 20 mils, respectively. The bottom sides of the two traces are 30 mils misaligned. The calculated impedance matrix is shown in Figure 5.18. The project file is saved under /examples/uneven_t.

```
Characteristic impedance in (Ohm), ignoring losses:
  6.39952e+001  1.45785e+001
  1.45785e+001  6.07730e+001
For nearly symmetric z-matrix
   Zcomm ~ (Z11+Z12)/2; Zdiff ~ 2*(Z11-Z12)
```

Figure 5.18: Impedance matrix of coupled microstrip traces with different thickness.

Chapter 6

File Formats

6.1 Layer Stackup File Format

User can specify the unit in the z-direction by a statement in form of

Unit unit_name

where unit_name can be one of the followings: {*in, cm, mm, mil, um, nm*}.

All materials used in a specific layer stackup have to be defined. A material definition is in form of

material material_name
type = conductor or insulator
er = value
tand = value
mr = value
sigma = value
;

where

- material_name: any name. But, it has to be in one word (containing no space)
- type: either "conductor" or "insulator"
- er: relative permittivity (a.k.a. dielectric constant)
- tanD: loss tangent
- mr: relative permeability
- sigma: conductivity in (S/m). It is important only for conductor, may use 0 for insulator

Then, the stackup file contains several interleaved dielectric and metal layer definition statements.

A dielectric layer is specified by

layer material_name
thickness = value
;

where material_name should be among the readily defined dielectric material names. thickness is a numerical value in z unit.

A metal layer is specified by

layer material_name
index = metal_layer_index
thickness = value
under_cut = value
trace_over_boundary = yes_or_no
 # between dielectric Layers n and (n+1)
z_offset = value
;

where material_name should be a readily defined conductor material names. metal_layer_index is an integer value (The top layer has index 1). thickness is a numerical value in z unit. yes_or_no for the "trace_over_boundary" attribute can be "yes" if the trace bottom side coincide with the dielectric layer boundary, or "no" if the trace top side align with the dielectric layer boundary. If the metal layer is a plane, it is represented by two consecutive lines of both "trace_over_boundary=yes", and "trace_over_boundary=no".

6.1.1 Example

```
# Tech file content
# generated by EE Circle TraceAnalyzer
# on 8-3-2007 at 2:38
# Unit
Unit um
# BEGIN material Er_3.25
material Er_3.25
 type = insulator
 er = 3.25
 tand = 0.02
 mr = 1.0
 sigma = 0.0
 ;
```

```
# END material Er_3.25
# BEGIN material Copper
material Copper
 type = conductor
 er = 1.0
 tand = 0.0
 mr = 1.0
 sigma = 7.0E7
 ;
# END material Copper
# BEGIN material air
material air
 type = insulator
 er = 1.0
 tand = 0.0
 mr = 1.0
 sigma = 0.0
 ;
# END material air
# BEGIN material FR4
material FR4
 type = insulator
 er = 4.2
 tand = 0.02
 mr = 1.0
 sigma = 0.0
 ;
# END material FR4
# 1: The 1-th dielectric layer
 layer air
 thickness = 10.0
 ;
# 2: The 1-th metal layer
 layer Copper
 index = 1
 thickness = 5.0
 under_cut = 0.0
 # constructed with entire_plane
```

```
 trace_over_boundary = yes
 trace_over_boundary = no
 # between dielectric Layers 1 and 2
 z_offset = 0.0
 ;
# 3: The 2-th dielectric layer
 layer Er_3.25
 thickness = 13.4
 ;
# 4: The 2-th metal layer
 layer Copper
 index = 2
 thickness = 1.4
 under_cut = 0.0
 trace_over_boundary = yes
 # between dielectric Layers 2 and 3
 z_offset = 0.0
 ;
# 5: The 3-th dielectric layer
 layer Er_3.25
 thickness = 12.0
 ;
# 6: The 3-th metal layer
 layer Copper
 index = 3
 thickness = 5.0
 under_cut = 0.0
 # constructed with entire_plane
 trace_over_boundary = yes
 trace_over_boundary = no
 # between dielectric Layers 3 and 4
 z_offset = 0.0
 ;
# 7: The 4-th dielectric layer
 layer air
 thickness = 10.0
 ;
```

6.2 Trace Definition File Format

User can specify the unit in the x-direction by a statement in form of

Unit unit_name

where unit_name can be one of the followings: {in, cm, mm, mil, um, nm}.

Next, the total number of traces is specified by a statement in form of

Num number_of_traces

Then, each trace is specified by

Trace metal_layer_index x_left width s_or_g;

where

- metal_layer_index: index of the metal layer
- x_left: x-coordinate of the left edge of the trace
- width: trace width
- s_or_g: use "g" if the trace is grounded. "s" for regular signal trace

6.2.1 Example

```
# Trace file
# generated by EE Circle Trace Analyzer
# on 8-3-2007 at 2:42
# Unit
Unit um
# Number of metal layers
Num 2
# Each line format: Trace layer_index x_coord width s/g
Trace 2 10.0 11.7 s;
Trace 2 28.1 11.7 s;
```

6.3 Using RLGC Data in ADS

Using the benchmark case of Section 4.2, suppose a file named "ms2.ads" is generated by Trace Analyzer using the "Export RLGC for ADS" menu. This file should be copied into the *data* subdirectory of the ADS project.

The content of the ADS-RLGC file is listed below:

```
BEGIN DSCR(RLGC)
! C[i][j]/eps0 L[i][j]/mu0 Rdc[i][j] Rhf[i][j]/sqrt(f_GHz) G[i][j]/omega*eps0
% C(real) L(real) Rdc(real) Rhf(real) G(real)
13.81562 0.25464 0.00000 0.02510 0.02874
-2.50049 0.08515 0.00000 0.00666 -0.03986
-2.50049 0.08515 0.00000 0.00666 -0.03986
13.81562 0.25464 0.00000 0.02510 0.02874
END
```

If the ADS version comes with a license for the "SPICE Translator" tool, then it might be possible to use even the HSPICE W-element model file directly. For users of ADS without the "SPICE Translator" option, there is a work-round to import RLGC file with the following procedure (the example given below was tested on version 2003c):

In the schematic editor, switch the design palate to "TLines-Multilayer", choose a "MLCTL_V" element with the matching topology as defined in TraceAnalyzer. In this example, a coupled two line component ML2CTL_V should be selected. Meanwhile, a substrate component, say, MLSUBSTRATE2 or any other substrate, is selected in order to have a valid ADS schematic design.

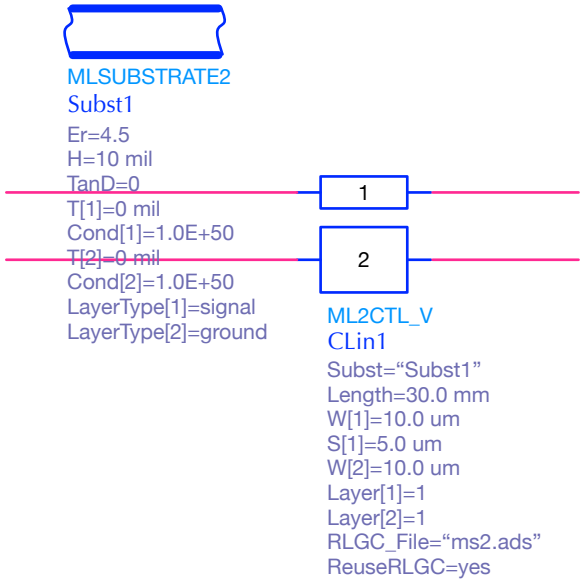

Figure 6.1: Using RLGC data inside an ADS design.

Double click on the ML2CTL_V component, to set the following fields correctly:

- Length=30.0 mm
- RLGC File="ms2.ads"
- ReuseRLGC=yes

Other parameters are left in their defaults since they will not affect the behavior of the 4-port structure. It is important to know that the file was located inside the data subdirectory under the current ADS project. Also, by choosing "ReuseRLGC=yes", all the geometry and layer definitions will be ignored. Obviously, the length parameter can be adjusted by the user to reflect the desired physical length.

> Be careful with the "ReuseRLGC" field. If it is accidentally set to "no", then the file "ms2.ads" will be overwritten by ADS in the next simulation, the file content will correlate to the geometry and layer parameters specified by the ML2CTL_V and MLSUBSTRATE2 components.

6.3.1 Time-Domain Verification of RLGC Parameters Generated by TraceAnalyzer in ADS

According to Trace Analyzer, the major characteristics of the coupled microstrip traces are:

Characteristic impedance in (Ohm), ignoring losses:

Even mode: 6.52991e+001, Common mode: 3.26495e+001

Odd mode: 3.84061e+001, Differential mode: 7.68122e+001

per-unit-length delay in (s/m), ignoring losses:

Mode1: 5.54575e-009

Mode2: 6.53898e-009

Now, the differential and common mode parameters with ADS transient simulations are shown in the figure below.

Marker m3 indicates the common-mode impedance of 32.287 (3.26495e+001 by Trace Analyzer). Marker m2 indicates the differential-mode impedance of 76.714 (7.68122e+001 by Trace Analyzer)

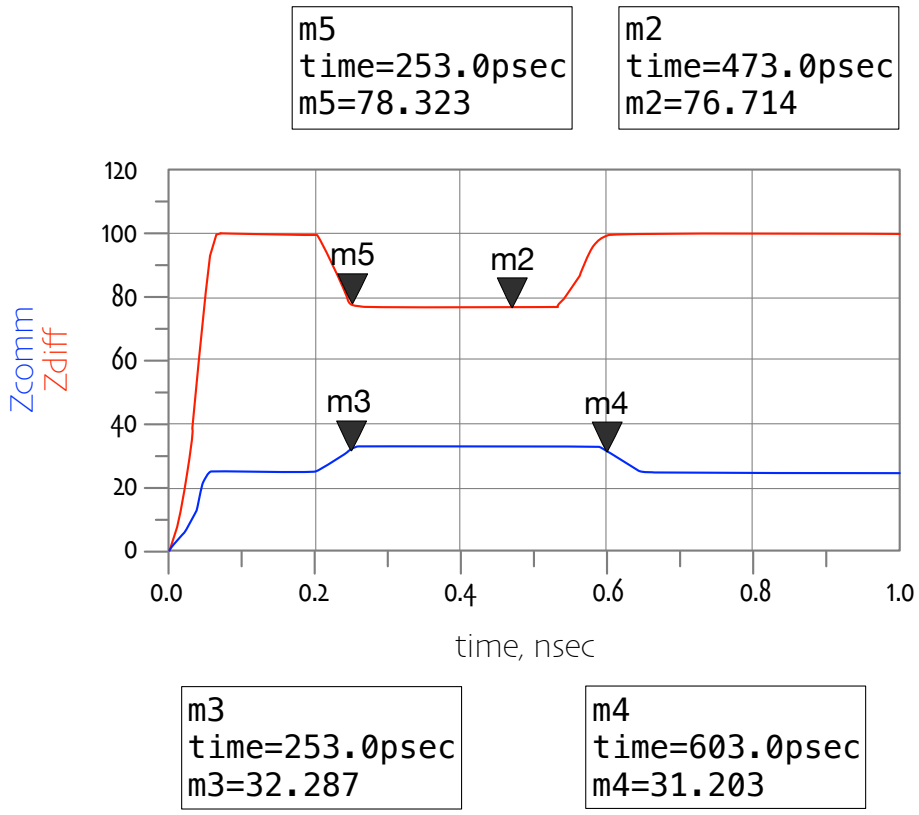

Figure 6.2: Time-domain verification of using RLGC data inside ADS.

The timing difference between markers m3 and m4 is 350 ps. For length of 30 mm and per-unit-length delay of 5.54575e-009 s/m (common-mode) calculated by Trace Analyzer, the total delay should be 2*0.03*5.54575e-009=3.32745e-10=332.7 ps, which is comparable to the Trace Analyzer result. Since there is a non-zero rise-time used in the transient simulation, the boundary of start and end points corresponding to the transmission-line terminals are somewhat difficult to determine.

Part II

Theoretical and Technical Notes

For advanced users, it is always beneficial to understand some of the "under-the-hood" details of the tool in order to be an expert. The problems addressed by this tool fall into a special category of the so-called multi-conductor transmission-line (MTL) structure in the layered dielectric media. For a system to be qualified as a transmission-line structure, there need to be at least two metal structures with uniform cross-sections. Electromagnetic (EM) waves can propagate along the metal lines. In particular, when the axial (or longitudinal) components of the EM fields vanish, the waves are in the so-called transverse electromagnetic (TEM) mode. Often, the axial components are not strictly zero, but are much smaller than the transverse components, resulting in the so-called quasi-TEM mode. The analyses of the tool assume quasi-TEM modes for all the traces being considered.

Theories and techniques of solving MTL system have been very mature [1], and widely embedded in many CAD or CAE tools. Two of the most popular techniques are the finite element method (FEM) and the method of moment (MOM), both formulated in the frequency domain. This tool is developed based on the MOM technique, which heavily relies on the evaluation of the Green's function in layered dielectric media. The following chapters cover only the MOM related techniques of solving the MTL problem.

Chapter 7

Multiconductor Transmission Line Theory

Assume that there are N_p planes, N_g traces connected to the ground (or GND in short) node that is always kept at zero potential ($\phi = 0$), and N signal traces. For the MTL system behave properly, it is necessary to have $N_p + N_g \geq 1$. In other words, there needs to be at least one conductor designated to be the reference conductor. Since the planes and the grounded traces by definition all have zero potential, only the voltages and current variables associated with the N signal traces are of interest in the MTL formulation.

7.1 Frequency-Domain MTL Equations

Denote

$$\begin{aligned} \mathbf{I} &= \left[\begin{array}{cccc} I_1 & I_2 & \cdots & I_N \end{array} \right]^T \\ \mathbf{V} &= \left[\begin{array}{cccc} V_1 & V_2 & \cdots & V_N \end{array} \right]^T \end{aligned}$$

to be the arrays of currents and voltages on the N signal traces. Let spatial variable x to represent the position along the direction of wave propagation. In general, all $\mathbf{I}/\mathbf{V}$ components are functions of x. Introducing four matrices ($\mathbf{R}_u, \mathbf{L}_u\mathbf{G}_u, \mathbf{C}_u$) of per-unit-length resistance, inductance, conductance, and capacitance quantities, the following matrix equations (generalized Telegrapher's Equations) describe the MTL system:

$$\begin{aligned} \frac{d}{dx}\mathbf{V}(x) &= -(\mathbf{R}_u + j\omega\mathbf{L}_u)\mathbf{I}(x), \\ \frac{d}{dx}\mathbf{I}(x) &= -(\mathbf{G}_u + j\omega\mathbf{C}_u)\mathbf{V}(x), \end{aligned}$$

where $\omega = 2\pi f$, is the angular frequency variable. A per-unit-length impedance matrix is defined as

$$\mathbf{Z}_u = \mathbf{R}_u + j\omega\mathbf{L}_u$$

and a per-unit-length admittance matrix is defined as

$$\mathbf{Y}_u = \mathbf{G}_u + j\omega\mathbf{C}_u.$$

Therefore, the system equations can also be written as

$$\begin{aligned} \frac{d}{dx}\mathbf{V}(x) &= -\mathbf{Z}_u\mathbf{I}(x), \\ \frac{d}{dx}\mathbf{I}(x) &= -\mathbf{Y}_u\mathbf{V}(x). \end{aligned}$$

7.2 Propagation Constant and Characteristic Impedance Matrices

At each frequency, matrices $\mathbf{P}_v$ and $\mathbf{P}_i$ and γ are defined by the following eigen-decompositions

$$\mathbf{Z}_u\mathbf{Y}_u = \mathbf{P}_v\gamma^2\mathbf{P}_v^{-1} \quad (7.1)$$
$$\mathbf{Y}_u\mathbf{Z}_u = \mathbf{P}_i\gamma^2\mathbf{P}_i^{-1} \quad (7.2)$$

where γ^2 is the diagonal matrix of all the eigenvalues. $\mathbf{P}_v$ is formed of scaled eigenvectors of $\mathbf{Z}_u\mathbf{Y}_u$, while $\mathbf{P}_i$ is formed of scaled eigenvectors of $\mathbf{Y}_u\mathbf{Z}_u$. The scaling constants can be determined [5] by

$$\mathbf{P}_i^\dagger\mathbf{P}_v = \mathbf{X} \quad (7.3)$$

and $\mathbf{X}$ has all its diagonal elements being 1's. In other words, the scalar-product of any column in $\mathbf{P}_i$ and the complex conjugate of the corresponding column in $\mathbf{P}_v$ is unity. Then, under the variable transformation of

$$\mathbf{V}_m(x) = \mathbf{P}_v^{-1}\mathbf{V}(x) \quad (7.4)$$
$$\mathbf{I}_m(x) = \mathbf{P}_i^{-1}\mathbf{I}(x) \quad (7.5)$$

then the original equations become

$$\frac{d}{dx}\mathbf{P}_v\mathbf{V}_m(x) = -\mathbf{Z}_u\mathbf{P}_i\mathbf{I}_m(x)$$
$$\frac{d}{dx}\mathbf{P}_i\mathbf{I}_m(x) = -\mathbf{Y}_u\mathbf{P}_v\mathbf{V}_m(x)$$

which is the modal form

$$\frac{d}{dx}\mathbf{V}_m(x) = -\mathbf{Z}_m\mathbf{I}_m(x)$$
$$\frac{d}{dx}\mathbf{I}_m(x) = -\mathbf{Y}_m\mathbf{V}_m(x) \quad (7.6)$$

where

$$\mathbf{Z}_m \equiv \mathbf{P}_v^{-1}\mathbf{Z}_u\mathbf{P}_i \quad (7.7)$$
$$\mathbf{Y}_m \equiv \mathbf{P}_i^{-1}\mathbf{Y}_u\mathbf{P}_v \quad (7.8)$$

whose components with units of (Ohm/m) and (1/Ohm/m), respectively. It's evident that

$$\mathbf{Z}_m\mathbf{Y}_m = \mathbf{Y}_m\mathbf{Z}_m = \gamma^2 \quad (7.9)$$

Besides the diagonal matrix of modal propagation constants γ, the modal characteristic impedance matrix can be introduced by

$$\mathbf{Z}_0 \equiv \sqrt{\mathbf{Z}_m \mathbf{Y}_m^{-1}} = \sqrt{\mathbf{Y}_m^{-1} \mathbf{Z}_m} \tag{7.10}$$

where all elements in have unit of Ohm. From (7.9) we have

$$\mathbf{Y}_m \mathbf{Z}_m \mathbf{Z}_m^{-2} = \gamma^2 \mathbf{Z}_m^{-2}$$

or

$$\mathbf{Z}_0^{-2} = \gamma^2 \mathbf{Z}_m^{-2} \tag{7.11}$$

Also

$$\mathbf{Z}_m \mathbf{Y}_m \mathbf{Y}_m^{-2} = \gamma^2 \mathbf{Y}_m^{-2}$$

or

$$\mathbf{Z}_0^2 = \gamma^2 \mathbf{Y}_m^{-2} \tag{7.12}$$

Then (7.11) and (7.12) imply

$$\mathbf{Z}_m = \gamma \mathbf{Z}_0 \tag{7.13}$$

$$\mathbf{Y}_m = \gamma \mathbf{Z}_0^{-1} \tag{7.14}$$

The governing equation for voltage is

$$\frac{d^2}{dx^2} \mathbf{V}_m(x) = \gamma^2 \mathbf{V}_m(x) \tag{7.15}$$

and for current is

$$\frac{d^2}{dx^2} \mathbf{I}_m(x) = \gamma^2 \mathbf{I}_m(x)$$

If we find the solution of $\mathbf{V}_m(x)$, then from (7.6) and (7.13)

$$\begin{aligned} \mathbf{I}_m(x) &= -\mathbf{Z}_m^{-1} \frac{d}{dx} \mathbf{V}_m(x) \\ &= -\left(\gamma \mathbf{Z}_0\right)^{-1} \frac{d}{dx} \mathbf{V}_m(x) \\ &= -\mathbf{Z}_0^{-1} \gamma^{-1} \frac{d}{dx} \mathbf{V}_m(x) \end{aligned}$$

i.e.

$$\mathbf{I}_m(x) = -\mathbf{Z}_0^{-1} \gamma^{-1} \frac{d}{dx} \mathbf{V}_m(x) \tag{7.16}$$

A theorem presented in [6] states:

Let Ξ and Υ be complex symmetric nonsingular matrices such that the eigenvalues of $\Xi\Upsilon$ are all distinct. Then and admit the unique simultaneous congruence decomposition

$$\begin{aligned}\Xi &= \mathbf{P}\delta_x\mathbf{P}^T \\ \Upsilon &= \mathbf{P}^{-T}\delta_y\mathbf{P}^{-1}\end{aligned}$$

where $\mathbf{P}$ is a non-singular matrix and δ_x, δ_y are diagonal matrices. This theorem can be applied for

$$\begin{aligned}\Xi &= \mathbf{Z}_u \\ \Upsilon &= \mathbf{Y}_u\end{aligned}$$

i.e., there exists $\mathbf{P}$ such that

$$\mathbf{Z}_u = \mathbf{P}\delta_z\mathbf{P}^T \tag{7.17}$$
$$\mathbf{Y}_u = \mathbf{P}^{-T}\delta_y\mathbf{P}^{-1} \tag{7.18}$$

Compared with (7.1) and (7.2) we have

$$\begin{aligned}\mathbf{P}_v &= \mathbf{P} \\ \mathbf{P}_i &= \mathbf{P}^{-T}\end{aligned}$$

and

$$\delta_z\delta_y = \gamma^2$$

using (7.17) and (7.18), then

$$\begin{aligned}\mathbf{Z}_m &= \mathbf{P}^{-1}\mathbf{Z}_u\mathbf{P}^{-T} = \mathbf{P}^{-1}\mathbf{P}\delta_z\mathbf{P}^T\mathbf{P}^{-T} = \delta_z \\ \mathbf{Y}_m &= \mathbf{P}_i^T\mathbf{Y}_u\mathbf{P} = \mathbf{P}_i^T\mathbf{P}^{-T}\delta_y\mathbf{P}^{-1}\mathbf{P} = \delta_y\end{aligned}$$

and

$$\mathbf{Z}_0 = \sqrt{\delta_z\delta_y^{-1}} = \sqrt{\delta_y^{-1}\delta_z}$$

Meanwhile

$$\begin{aligned}&\mathbf{Y}_u^{-1}\sqrt{\mathbf{Y}_u\mathbf{Z}_u} \\ =\ &\left(\mathbf{P}^{-T}\delta_y\mathbf{P}^{-1}\right)^{-1}\sqrt{\mathbf{P}^{-T}\delta_y\mathbf{P}^{-1}\mathbf{P}\delta_z\mathbf{P}^T} \\ =\ &\mathbf{P}\delta_y^{-1}\mathbf{P}^T\mathbf{P}^{-T}\sqrt{\delta_y\delta_z}\mathbf{P}^T \\ =\ &\mathbf{P}\sqrt{\delta_y^{-1}\delta_z}\mathbf{P}^T = \mathbf{P}\mathbf{Z}_0\mathbf{P}^T\end{aligned}$$

and

$$\begin{aligned}
& \mathbf{Z}_u(\sqrt{\mathbf{Y}_u\mathbf{Z}_u})^{-1} \\
= \; & \mathbf{P}\delta_z\mathbf{P}^T(\sqrt{\mathbf{P}^{-T}\delta_y\mathbf{P}^{-1}\mathbf{P}\delta_z\mathbf{P}^T})^{-1} \\
= \; & \mathbf{P}\delta_z\mathbf{P}^T\left[\mathbf{P}^{-T}\left(\delta_y\delta_z\right)^{-\frac{1}{2}}\mathbf{P}^T\right] \\
= \; & \mathbf{P}\delta_z\left(\delta_z^{-\frac{1}{2}}\delta_y^{-\frac{1}{2}}\right)\mathbf{P}^T \\
= \; & \mathbf{P}\sqrt{\delta_z\delta_y^{-1}}\mathbf{P}^T = \mathbf{P}\mathbf{Z}_0\mathbf{P}^T
\end{aligned}$$

These results enable us to define a non-modal characteristic impedance matrix as

$$\mathbf{Z}_C \equiv \mathbf{P}\mathbf{Z}_0\mathbf{P}^T = \mathbf{Y}_u^{-1}\sqrt{\mathbf{Y}_u\mathbf{Z}_u} = \mathbf{Z}_u(\sqrt{\mathbf{Y}_u\mathbf{Z}_u})^{-1} \tag{7.19}$$

which in general have non-zero off-diagonal elements. In fact, (7.19) is implemented in Trace Analyzer for reporting the characteristic impedance matrix. When $N = 1$, for a single trace, the propagation constant and the characteristic impedance take the familiar forms of

$$\begin{aligned}
\gamma &= \sqrt{Y_uZ_u} = \sqrt{(R + j\omega L)(G + j\omega C)} \\
Z_C &= \sqrt{\frac{Z_u}{Y_u}} = \sqrt{\frac{R + j\omega L}{G + j\omega C}}.
\end{aligned}$$

7.3 Balanced Lossless Coupled Lines

When $N = 2$, a pair of unbalanced lossless coupled line are characterized by

$$\mathbf{L}_u = \begin{bmatrix} L & M \\ M & L \end{bmatrix} \tag{7.20}$$

$$\mathbf{C}_u = \begin{bmatrix} C & -C_m \\ -C_m & C \end{bmatrix} \tag{7.21}$$

Then

$$\begin{aligned} \mathbf{Z}_u &= j\omega \mathbf{L}_u \\ \mathbf{Y}_u &= j\omega \mathbf{C}_u \end{aligned}$$

It can be shown that

$$\mathbf{Z}_u \mathbf{Y}_u = -\omega^2 \mathbf{L}_u \mathbf{C}_u = \mathbf{P}_v \begin{bmatrix} -\omega^2 (L-M)(C+C_m) & 0 \\ 0 & -\omega^2 (L+M)(C-Cm) \end{bmatrix} \mathbf{P}_v^{-1}$$

where

$$\begin{aligned} \mathbf{P}_v &= \begin{bmatrix} 1 & 1 \\ -1 & 1 \end{bmatrix} \\ \mathbf{P}_v^{-1} &= \frac{1}{2} \begin{bmatrix} 1 & -1 \\ 1 & 1 \end{bmatrix} \end{aligned}$$

Also,

$$\mathbf{Y}_u \mathbf{Z}_u = -\omega^2 \mathbf{C}_u \mathbf{L}_u = \mathbf{P}_i \begin{bmatrix} -\omega^2 (L-M)(C+C_m) & 0 \\ 0 & -\omega^2 (L+M)(C-Cm) \end{bmatrix} \mathbf{P}_i^{-1}$$

where

$$\begin{aligned} \mathbf{P}_i &= \begin{bmatrix} 1 & 1 \\ -1 & 1 \end{bmatrix} \\ \mathbf{P}_i^{-1} &= \frac{1}{2} \begin{bmatrix} 1 & -1 \\ 1 & 1 \end{bmatrix} \end{aligned}$$

Obviously, we have

$$\gamma^2 \equiv \begin{bmatrix} \gamma_o^2 & 0 \\ 0 & \gamma_e^2 \end{bmatrix} = \begin{bmatrix} -\omega^2 (L-M)(C+C_m) & 0 \\ 0 & -\omega^2 (L+M)(C-Cm) \end{bmatrix}$$

consequently, the odd- and even-mode propagation constants are defined as

$$\gamma_o \equiv j\beta_o = j\omega\sqrt{(L-M)(C+C_m)} \tag{7.22}$$
$$\gamma_e \equiv j\beta_e = j\omega\sqrt{(L+M)(C-Cm)} \tag{7.23}$$

In balanced system, the eigenvector matrices are identical, we may drip the subscript, i.e.

$$\mathbf{P} \equiv \mathbf{P}_v = \mathbf{P}_i$$

For each mode, other wave parameters can be derived by

- Wavelength: $\lambda = \frac{2\pi}{\beta}$
- Propagation velocity: $v = \frac{\omega}{\beta}$
- Effective dielectric constant: $K = \left(\frac{\beta c_0}{\omega}\right)^2$

Now, using the eigen-decomposition results, we have

$$\begin{aligned}\mathbf{Z}_m &= \mathbf{P}_v^{-1}\mathbf{Z}_u\mathbf{P}_i = j\omega\mathbf{P}_v^{-1}\mathbf{L}_u\mathbf{P}_i = j\omega\begin{bmatrix} L-M & 0 \\ 0 & L+M \end{bmatrix} \\ &= \gamma\mathbf{Z}_0 = j\omega\begin{bmatrix} \sqrt{(L-M)(C+C_m)} & 0 \\ 0 & \sqrt{(L+M)(C-Cm)} \end{bmatrix}\mathbf{Z}_0\end{aligned}$$

thus if we force the characteristic impedance matrix to be diagonal

$$\mathbf{Z}_0 \equiv \begin{bmatrix} Z_o & 0 \\ 0 & Z_e \end{bmatrix} = \begin{bmatrix} \sqrt{\frac{L-M}{C+C_m}} & 0 \\ 0 & \sqrt{\frac{L+M}{C-C_m}} \end{bmatrix}$$

which implies

$$Z_o = \sqrt{\frac{L-M}{C+C_m}} \tag{7.24}$$
$$Z_e = \sqrt{\frac{L+M}{C-C_m}} \tag{7.25}$$

In a source-free region, the modal equation for voltage is (7.4), or

$$\frac{d^2}{dx^2}\mathbf{V}_m(x) = \gamma^2\mathbf{V}_m(x)$$

which has the solution of

$$\mathbf{V}_m(x) \equiv \begin{bmatrix} V_o(x) \\ V_e(x) \end{bmatrix} = \begin{bmatrix} A_o e^{-j\beta_o x} + B_o e^{j\beta_o x} \\ A_e e^{-j\beta_e x} + B_e e^{j\beta_e x} \end{bmatrix}$$

and by (7.16)

$$\begin{aligned} \mathbf{I}_m(x) &= -\mathbf{Z}_0^{-1}\gamma^{-1}\frac{d}{dx}\mathbf{V}_m(x) \\ &= -\begin{bmatrix} Z_o^{-1} & 0 \\ 0 & Z_e^{-1} \end{bmatrix}\begin{bmatrix} j\beta_o & 0 \\ 0 & j\beta_o \end{bmatrix}^{-1}\begin{bmatrix} -j\beta_o\left(A_o e^{-j\beta_o x} - B_o e^{j\beta_o x}\right) \\ -j\beta_e\left(A_e e^{-j\beta_e x} - B_e e^{j\beta_e x}\right) \end{bmatrix} \\ &= \begin{bmatrix} Z_o^{-1}\left(A_o e^{-j\beta_o x} - B_o e^{j\beta_o x}\right) \\ Z_e^{-1}\left(A_e e^{-j\beta_e x} - B_e e^{j\beta_e x}\right) \end{bmatrix} \end{aligned}$$

According to (7.4) and (7.5), the modal voltage/current vectors are related to the singled-ended quantities by

$$\begin{aligned} \mathbf{V}(x) &\equiv \begin{bmatrix} V_P(x) \\ V_N(x) \end{bmatrix} = \mathbf{P}_v\mathbf{V}_m(x) = \begin{bmatrix} 1 & 1 \\ -1 & 1 \end{bmatrix}\begin{bmatrix} A_o e^{-j\beta_o x} + B_o e^{j\beta_o x} \\ A_e e^{-j\beta_e x} + B_e e^{j\beta_e x} \end{bmatrix} \\ \mathbf{I}(x) &\equiv \begin{bmatrix} I_P(x) \\ I_N(x) \end{bmatrix} = \mathbf{P}_i\mathbf{I}_m(x) = \begin{bmatrix} 1 & 1 \\ -1 & 1 \end{bmatrix}\begin{bmatrix} Z_o^{-1}\left(A_o e^{-j\beta_o x} - B_o e^{j\beta_o x}\right) \\ Z_e^{-1}\left(A_e e^{-j\beta_e x} - B_e e^{j\beta_e x}\right) \end{bmatrix} \end{aligned}$$

In other words, the general solutions are

$$\begin{aligned} V_P(x) &= A_o e^{-j\beta_o x} + B_o e^{j\beta_o x} + A_e e^{-j\beta_e x} + B_e e^{j\beta_e x} \\ V_N(x) &= -\left(A_o e^{-j\beta_o x} + B_o e^{j\beta_o x}\right) + \left(A_e e^{-j\beta_e x} + B_e e^{j\beta_e x}\right) \\ I_P(x) &= Z_o^{-1}\left(A_o e^{-j\beta_o x} - B_o e^{j\beta_o x}\right) + Z_e^{-1}\left(A_e e^{-j\beta_e x} - B_e e^{j\beta_e x}\right) \\ I_N(x) &= -Z_o^{-1}\left(A_o e^{-j\beta_o x} - B_o e^{j\beta_o x}\right) + Z_e^{-1}\left(A_e e^{-j\beta_e x} - B_e e^{j\beta_e x}\right) \end{aligned}$$

Conversely,

$$\begin{aligned} \begin{bmatrix} V_o(x) \\ V_e(x) \end{bmatrix} &= \mathbf{P}^{-1}\begin{bmatrix} V_P(x) \\ V_N(x) \end{bmatrix} \\ \begin{bmatrix} I_o(x) \\ I_e(x) \end{bmatrix} &= \mathbf{P}^{-1}\begin{bmatrix} I_P(x) \\ I_N(x) \end{bmatrix} \end{aligned}$$

In other words, the modal voltage/current variables are related to their single-ended versions by

$$\begin{aligned} V_o(x) &= \frac{1}{2}\left[V_P(x) - V_N(x)\right] \\ V_e(x) &= \frac{1}{2}\left[V_P(x) + V_N(x)\right] \\ I_o(x) &= \frac{1}{2}\left[I_P(x) - I_N(x)\right] \\ I_e(x) &= \frac{1}{2}\left[I_P(x) + I_N(x)\right] \end{aligned}$$

7.4 Slightly Unbalanced Lossless Coupled Lines

When $N = 2$, a pair of unbalanced lossless coupled line are characterized by

$$\begin{aligned}\mathbf{L}_u &= \begin{bmatrix} L - \frac{1}{2}\Delta L & M \\ M & L + \frac{1}{2}\Delta L \end{bmatrix} \\ \mathbf{C}_u &= \begin{bmatrix} C + \frac{1}{2}\Delta C & -C_m \\ -C_m & C - \frac{1}{2}\Delta C \end{bmatrix}\end{aligned}$$

Then

$$\begin{aligned}\mathbf{Z}_u &= j\omega\mathbf{L}_u \\ \mathbf{Y}_u &= j\omega\mathbf{C}_u\end{aligned}$$

It can be shown that

$$\mathbf{Z}_u\mathbf{Y}_u = -\omega^2\mathbf{L}_u\mathbf{C}_u = \mathbf{P}_v \begin{bmatrix} -\omega^2 (L - M)(C + C_m) & 0 \\ 0 & -\omega^2 (L + M)(C - Cm) \end{bmatrix} \mathbf{P}_v^{-1}$$

where

$$\begin{aligned}\mathbf{P}_v &\approx \begin{bmatrix} 1 & 1 \\ -1 + \frac{1}{2}(\xi + \eta) & 1 + \frac{1}{2}(\xi - \eta) \end{bmatrix} \\ \mathbf{P}_v^{-1} &\approx \frac{1}{2}\begin{bmatrix} 1 + \frac{1}{2}\xi & -\left(1 + \frac{1}{2}\eta\right) \\ 1 - \frac{1}{2}\xi & 1 + \frac{1}{2}\eta \end{bmatrix}\end{aligned}$$

with

$$\xi \equiv \frac{C\Delta L - L\Delta C}{CM - LC_m} \tag{7.26}$$

$$\eta \equiv \frac{C_m\Delta L - M\Delta C}{CM - LC_m} \tag{7.27}$$

Likewise

$$\mathbf{Y}_u\mathbf{Z}_u = -\omega^2\mathbf{C}_u\mathbf{L}_u = \mathbf{P}_i \begin{bmatrix} -\omega^2 (L - M)(C + C_m) & 0 \\ 0 & -\omega^2 (L + M)(C - Cm) \end{bmatrix} \mathbf{P}_i^{-1}$$

where

$$\begin{aligned}\mathbf{P}_i &\approx \begin{bmatrix} 1 & 1 \\ -1 + \frac{1}{2}(\xi - \eta) & 1 + \frac{1}{2}(\xi + \eta) \end{bmatrix} \\ \mathbf{P}_i^{-1} &\approx \frac{1}{2}\begin{bmatrix} 1 + \frac{1}{2}\xi & -\left(1 - \frac{1}{2}\eta\right) \\ 1 - \frac{1}{2}\xi & 1 - \frac{1}{2}\eta \end{bmatrix}\end{aligned}$$

Obviously, we have

$$\gamma^2 \equiv \begin{bmatrix} \gamma_o^2 & 0 \\ 0 & \gamma_e^2 \end{bmatrix} = \begin{bmatrix} -\omega^2 (L-M)(C+C_m) & 0 \\ 0 & -\omega^2 (L+M)(C-Cm) \end{bmatrix}$$

consequently, the odd- and even-mode propagation constants are the same as in (7.22) and (7.23). For each mode, other wave parameters can be derived by

- Wavelength: $\lambda = \frac{2\pi}{\beta}$
- Propagation velocity: $v = \frac{\omega}{\beta}$
- Effective dielectric constant: $K = \left(\frac{\beta c_0}{\omega}\right)^2$

Now, using the eigen-decomposition results, we have

$$\begin{aligned} \mathbf{Z}_m &= \mathbf{P}_v^{-1}\mathbf{Z}_u\mathbf{P}_i = j\omega\mathbf{P}_v^{-1}\mathbf{L}_u\mathbf{P}_i \approx j\omega \begin{bmatrix} \frac{(\xi+2)(L-M)}{2+\xi-\eta} & \frac{-\xi M+\eta L+\Delta L}{2-\xi-\eta} \\ \frac{\xi M-\eta L-\Delta L}{2+\xi-\eta} & \frac{(2-\xi)(L+M)}{2-\xi-\eta} \end{bmatrix} \\ &= \gamma\mathbf{Z}_0 = j\omega \begin{bmatrix} \sqrt{(L-M)(C+C_m)} & 0 \\ 0 & \sqrt{(L+M)(C-Cm)} \end{bmatrix} \mathbf{Z}_0 \end{aligned}$$

thus if we force the characteristic impedance matrix to be diagonal

$$\mathbf{Z}_0 \equiv \begin{bmatrix} Z_o & 0 \\ 0 & Z_e \end{bmatrix} \approx \begin{bmatrix} \frac{2+\xi}{2+\xi-\eta}\sqrt{\frac{L-M}{C+C_m}} & 0 \\ 0 & \frac{2-\xi}{2-\xi-\eta}\sqrt{\frac{L+M}{C-C_m}} \end{bmatrix} \approx \begin{bmatrix} \left(1+\frac{1}{2}\eta\right)\sqrt{\frac{L-M}{C+C_m}} & 0 \\ 0 & \left(1+\frac{1}{2}\eta\right)\sqrt{\frac{L+M}{C-C_m}} \end{bmatrix}$$

which implies

$$\begin{aligned} Z_o &= \frac{2+\xi}{2+\xi-\eta}\sqrt{\frac{L-M}{C+C_m}} \\ Z_e &= \frac{2-\xi}{2-\xi-\eta}\sqrt{\frac{L+M}{C-C_m}} \end{aligned}$$

In a source-free region, the modal equation for voltage is (7.15), or

$$\frac{d^2}{dx^2}\mathbf{V}_m(x) = \gamma^2\mathbf{V}_m(x)$$

which has the solution of

$$\mathbf{V}_m(x) \equiv \begin{bmatrix} V_o(x) \\ V_e(x) \end{bmatrix} = \begin{bmatrix} A_o e^{-j\beta_o x} + B_o e^{j\beta_o x} \\ A_e e^{-j\beta_e x} + B_e e^{j\beta_e x} \end{bmatrix}$$

and by (7.16)

$$\begin{aligned}
\mathbf{I}_m(x) &= -\mathbf{Z}_0^{-1}\gamma^{-1}\frac{d}{dx}\mathbf{V}_m(x) \\
&= -\begin{bmatrix} Z_o^{-1} & 0 \\ 0 & Z_e^{-1} \end{bmatrix}\begin{bmatrix} j\beta_o & 0 \\ 0 & j\beta_o \end{bmatrix}^{-1}\begin{bmatrix} -j\beta_o\left(A_o e^{-j\beta_o x} - B_o e^{j\beta_o x}\right) \\ -j\beta_e\left(A_e e^{-j\beta_e x} - B_e e^{j\beta_e x}\right) \end{bmatrix} \\
&= \begin{bmatrix} Z_o^{-1}\left(A_o e^{-j\beta_o x} - B_o e^{j\beta_o x}\right) \\ Z_e^{-1}\left(A_e e^{-j\beta_e x} - B_e e^{j\beta_e x}\right) \end{bmatrix}
\end{aligned}$$

According to (7.4) and (7.5), the modal voltage/current vectors are related to the singled-ended quantities by

$$\begin{aligned}
\mathbf{V}(x) &\equiv \begin{bmatrix} V_P(x) \\ V_N(x) \end{bmatrix} = \mathbf{P}_v\mathbf{V}_m(x) \approx \begin{bmatrix} 1 & 1 \\ -1+\frac{1}{2}(\xi+\eta) & 1+\frac{1}{2}(\xi-\eta) \end{bmatrix}\begin{bmatrix} A_o e^{-j\beta_o x} + B_o e^{j\beta_o x} \\ A_e e^{-j\beta_e x} + B_e e^{j\beta_e x} \end{bmatrix} \\
\mathbf{I}(x) &\equiv \begin{bmatrix} I_P(x) \\ I_N(x) \end{bmatrix} = \mathbf{P}_i\mathbf{I}_m(x) \approx \begin{bmatrix} 1 & 1 \\ -1+\frac{1}{2}(\xi-\eta) & 1+\frac{1}{2}(\xi+\eta) \end{bmatrix}\begin{bmatrix} Z_o^{-1}\left(A_o e^{-j\beta_o x} - B_o e^{j\beta_o x}\right) \\ Z_e^{-1}\left(A_e e^{-j\beta_e x} - B_e e^{j\beta_e x}\right) \end{bmatrix}
\end{aligned}$$

In other words, the general solutions are

$$\begin{aligned}
V_P(x) &\approx A_o e^{-j\beta_o x} + B_o e^{j\beta_o x} + A_e e^{-j\beta_e x} + B_e e^{j\beta_e x} \\
V_N(x) &\approx \left[-1+\frac{1}{2}(\xi+\eta)\right]\left(A_o e^{-j\beta_o x} + B_o e^{j\beta_o x}\right) + \left[1+\frac{1}{2}(\xi-\eta)\right]\left(A_e e^{-j\beta_e x} + B_e e^{j\beta_e x}\right) \\
I_P(x) &\approx Z_o^{-1}\left(A_o e^{-j\beta_o x} - B_o e^{j\beta_o x}\right) + Z_e^{-1}\left(A_e e^{-j\beta_e x} - B_e e^{j\beta_e x}\right) \\
I_N(x) &\approx \left[-1+\frac{1}{2}(\xi-\eta)\right]Z_o^{-1}\left(A_o e^{-j\beta_o x} - B_o e^{j\beta_o x}\right) + \left[1+\frac{1}{2}(\xi+\eta)\right]Z_e^{-1}\left(A_e e^{-j\beta_e x} - B_e e^{j\beta_e x}\right)
\end{aligned}$$

Now,

$$\frac{V_P(x) - V_N(x)}{2} \approx \left[1-\frac{1}{4}(\xi+\eta)\right]\left(A_o e^{-j\beta_o x} + B_o e^{j\beta_o x}\right) - \frac{1}{2}(\xi-\eta)\left(A_e e^{-j\beta_e x} + B_e e^{j\beta_e x}\right) \quad (7.28)$$

$$\frac{V_P(x) + V_N(x)}{2} \approx \frac{1}{2}(\xi+\eta)\left(A_o e^{-j\beta_o x} + B_o e^{j\beta_o x}\right) + \left[1+\frac{1}{4}(\xi-\eta)\right]\left(A_e e^{-j\beta_e x} + B_e e^{j\beta_e x}\right) \quad (7.29)$$

Based on this result, in a slightly unbalanced coupled pair, the rough estimate of the modal conversion factor is

$$\frac{1}{2}\max\left\{|\xi-\eta|, |\xi+\eta|\right\}$$

7.5 Crosstalk Characterization

In Young's book [7], for two balanced coupled lines with per-uni-length L/C matrices of (7.20) and (7.21), the normalized near-end coupling ratio is

$$K_{NE,peak,matched} = \frac{1}{4}\left(\frac{C_m}{C} + \frac{M}{L}\right)$$

while the far-end noise voltage is related to the time-derivative of the source

$$V_{FE,peak} = \frac{l}{2}\left(\sqrt{\frac{L}{C}}C_m - \sqrt{\frac{C}{L}}M\right)\frac{dv_s}{dt}$$

And if the time-derivative of the aggressor is approximated by $\frac{V_a}{t_t}$, as in [8], the far-end crosstalk becomes

$$V_{FE,peak} = \frac{l}{2}\sqrt{LC}\left(\frac{C_m}{C} - \frac{M}{L}\right)\frac{V_a}{t_r}$$

However, more general formulas are found in [9] with aggressor on Line-1, for victim on Line-2

$$\begin{aligned} V_{NE}(t) &= \frac{1}{8\sqrt{L_{11}C_{11}}}\left(\sqrt{\frac{L_{22}}{C_{22}}}\,|C_{12}| + \sqrt{\frac{C_{11}}{L_{11}}}L_{12}\right)[V_s(t) - V_s(t-2T)] \\ V_{FE}(t) &= \frac{l}{4}\left(\sqrt{\frac{L_{22}}{C_{22}}}\,|C_{12}| - \sqrt{\frac{C_{11}}{L_{11}}}L_{12}\right)\frac{d}{dt}V_s(t-T) \end{aligned}$$

where T is the one-way delay of the lines. Thus, the normalized coupling coefficients are

$$\begin{aligned} K_{NE,1\to2} &= \sqrt{\frac{L_{22}}{L_{11}C_{11}C_{22}}}\,|C_{12}| + \frac{L_{12}}{L_{11}} \\ K_{FE,1\to2}t_r &= \sqrt{\frac{L_{22}}{C_{22}}}\,|C_{12}| - \sqrt{\frac{C_{11}}{L_{11}}}L_{12} \end{aligned}$$

Replacing indices $1, 2$ with i, j and take the worst-case value, we have

$$K_{NE,i\to j} = \sqrt{\frac{L_{jj}}{L_{ii}C_{ii}C_{jj}}}\,|C_{ij}| + \frac{L_{ij}}{L_{ii}} \tag{7.30}$$

$$K_{FE,i\to j}t_r = \sqrt{\frac{L_{jj}}{C_{jj}}}\,|C_{ij}| - \sqrt{\frac{C_{ii}}{L_{ii}}}L_{ij} \tag{7.31}$$

The definitions of (7.30) and (7.31) are implemented in Trace Analyzer for K_{NE} (unit-less) and K_{FE} (with unit of s/m) matrices where only the off-diagonal elements are meaningful.

Chapter 8

Techniques of Finding the RLGC Parameters of MTL

The most important parameter is the per-unit-length capacitance matrix. Once the procedure of finding **C** is developed, the rest of the parameters can be derived.

8.1 Computing the L Matrix

Once the procedure of computing **C** matrix is established, a special capacitance matrix, $\mathbf{C}_0$, associated with the same set of traces with dielectric layers removed (left with vacuum), can be easily computed. The inductance matrix for a non-magnetic media is given by [10]

$$\mathbf{L} = \mu_0 \epsilon_0 \mathbf{C}_0^{-1}.$$

When there are magnetic materials in some layers, the inductance matrix can be determined by [11]

$$\mathbf{L} = \mu_0 \epsilon_0 \mathbf{C}_{R,0}^{-1}.$$

where the $\mathbf{C}_{R,0}$ matrix is computed by assigning the relative dielectric constant of each magnetic layer as

$$\epsilon_r = \mu_r^{-1}.$$

8.2 Computing the R Matrix

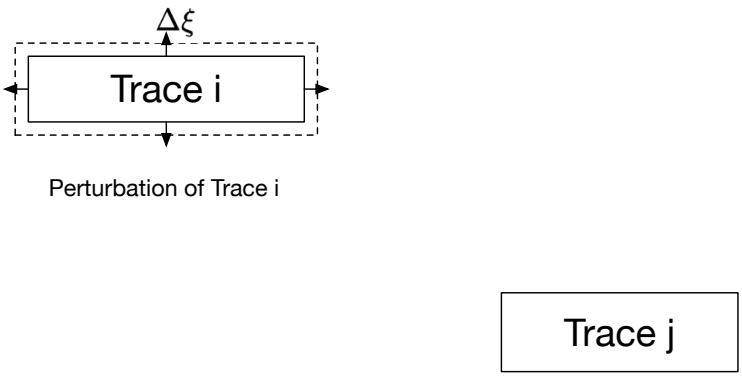

Figure 8.1: Scheme of computing skin resistance matrix.

The resistance matrix can be broken into two parts: $\mathbf{R}_0$ of DC resistance, and R_s caused by the skin effect. Assuming σ to be the conductivity of the trace metal, the terms of $\mathbf{R}_0$ are simply given by the Ohm's law as

$$R_{0,ij} = \begin{cases} \frac{1}{\sigma w_i t_i}, & i = j \\ 0, & \text{otherwise} \end{cases}$$

where w_i and t_i are the width and thickness of Trace i, respectively. The terms of skin resistance are computed following the Wheeler's rule [12] by perturbing Trace i (expanding its surface outward by a distance of $\Delta\xi$ along the surface normal directions) and compute the inductance matrices before and after the perturbation:

$$R_{s,ij} = -\sqrt{\frac{\pi f}{\mu\sigma}} \frac{L_{ij}^{after} - L_{ij}^{before}}{\Delta\xi}.$$

8.3 Computing the $\mathbf{G_d}$ Matrix

The conductance matrix consists of two parts

$$\mathbf{G} = \mathbf{G}_0 + \mathbf{G}_d$$

where $\mathbf{G}_d$ is caused by the dielectric loss, and $\mathbf{G}_0$ contains leakages by other mechanisms. Ordinarily, $\mathbf{G}_0 = 0$. The dielectric-based conductance matrix can be obtained by using the complex permittivity values for each dielectric layer

$$\epsilon = \epsilon_r(1 - j\tan\delta).$$

Going through the complex-valued matrix algebra, the resultant capacitance matrix, $\hat{\mathbf{C}}$, is also complex-valued. Then splitting the real and imaginary parts, with

$$\mathbf{C} = \Re\{\hat{\mathbf{C}}\}$$

and the conductance matrix is simply

$$\mathbf{G}_d = -\omega\Im\{\hat{\mathbf{C}}\}.$$

Chapter 9

Calculation of the Capacitance Matrix in Trace Analyzer

9.1 Green's Function in Layered Media

The scalar potential function $\phi(x, z)$ can be expressed in terms of the charge density $\sigma(x', z')$ and the 2D spatial Green's function $G^{\phi}(x, x'; z, z')$ by

$$\phi(x, z) = \int_C \sigma(x', z') G^{\phi}(x, x'; z, z') d\xi \tag{9.1}$$

where path C encompasses all boundaries of metal objects. The 2D spatial Green's function is derived from the 3D spectral Green's function $\tilde{G}(\gamma; z, z')$ by [13]

$$G^{\phi}(x, x'; z, z') = \frac{1}{2\pi} \int_{-\infty}^{\infty} \tilde{G}^{\phi}(\gamma, z, z') e^{j\gamma(x-x')} d\gamma. \tag{9.2}$$

The spectral Green's function satisfies

$$\left(\frac{\partial^2}{\partial z^2} + k_z^2 \right) \tilde{G}^{\phi}(x, x'; z, z') = -\delta(z - z').$$

Bookkeeping for a multi-layered structure

A general multi-layered dielectric stackup is comprised of a sequence of n dielectric slabs stacked along the vertical or z-direction. It is assumed that each dielectric slab has infinite extent in the lateral xy-plane to simplify the calculations. There are variations in the book-keeping methods for such structures: (1) The positive $\hat{z}$ can be defined either upward or downward; (2) The material indexing can be either increasing or decreasing along the $\hat{z}$ direction; (3) The global vertical

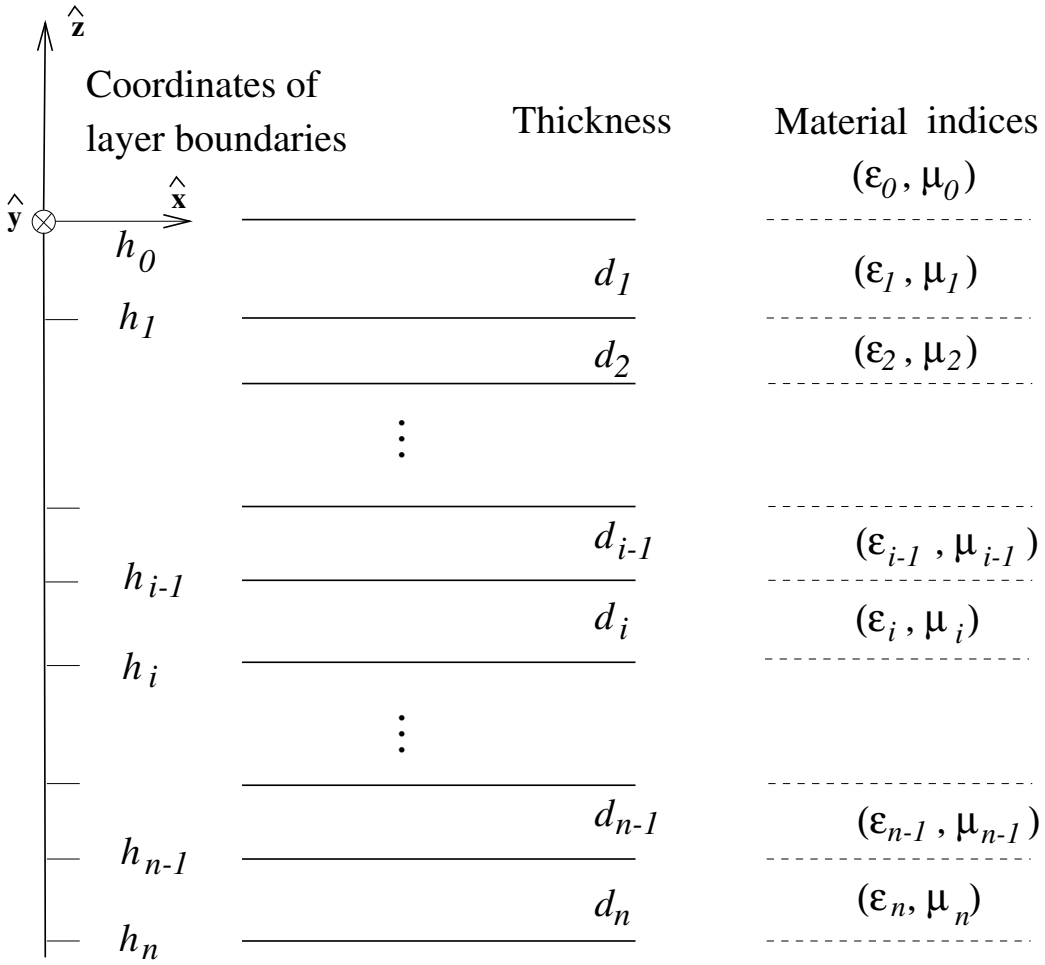

Figure 9.1: Description of dielectric layers with infinite lateral extent (in x, y directions). Either the top or the bottom side may be terminated by a perfect electric conductor (PEC).

reference location for $z = 0$ can be fixed within a particular layer or can be flexible. All three factors affect the expressions of the spectral Green's functions. A scheme that is most suitable to the multilayered PCB/package design convention is adopted here and illustrated in Figure 9.1:

- The $+\hat{z}$ direction points upward;
- The material index starts from 0 and increases along the $-\hat{z}$ direction;
- The global $z = 0$ reference is flexible in all derivations of $\tilde{G}^{\phi}$. But eventually the $z = 0$ reference shall be chosen in computation. It is suggested that the $z = 0$ location be the boundary between the 0-th and the 1st materials, implying $h_0 = 0$.
- Then all boundaries between the neighboring slabs are given by

$$h_i = h_{i-1} - d_i \text{ for } i = 1..n \tag{9.3}$$

  where d_i is the thickness of the ith layer.

9.2 The spectral-domain Green's functions

The spectral Green's functions in simple layered-structures such as microstrip and stripline are well known [14, 15]. For structures involving three layers, the static Green's function can also be found in the literature [16]. All the necessary equations that can be applied to the derivation of spectral Green's functions in a general multilayered structure are given in Chew's book [17]. Chow *et al.* [18, 19] recognized that the spectral Green's functions can be approximated by a series of complex images using the well-known Prony's method. One research group led by Askun has devoted tremendous effort to the subject of computing the so-called closed-form spatial Green's functions in general layered media [20, 21, 22, 23, 24] where the key is the improvement of the Prony's method – a numerical technique called the generalized pencil of function (GPOF) first introduced by Hua [25, 26]. The spectral Green's functions $\tilde{G}^{\phi}$ were found in complete and efficient forms by Tsai [27]. Detailed steps suitable for computer implementation are given toward the derivation of the spectral Green's functions based on the information from all the above references.

9.2.1 Generalized Reflection Coefficients

The spectral Green's functions are expressed in terms of many coefficients which should be calculated first. Assume the frequency f and $\omega = 2\pi f$ is set. With iterations taken through $p, j = 1..n$ for the index of the field-point layer, the wave number in the p-th layer is

$$k_p = \omega\sqrt{\epsilon_p \mu_p}, \tag{9.4}$$

and the propagation constant along the z-direction can be defined by either

$$k_{zj} = \sqrt{k_j^2 - k_\rho^2} \tag{9.5}$$

or

$$\gamma_j = jk_{zj} = \sqrt{k_\rho^2 - k_j^2} \tag{9.6}$$

where

$$k_\rho^2 = k_x^2 + k_y^2 \tag{9.7}$$

is invariant with respect to index j due to the phase-matching boundary conditions [28]. In the above equations, j has been used as both an layer index and $\sqrt{-1}$. It is advantageous to use γ_j instead of k_{zj} to avoid confusion. The complex square-root operation is multi-valued [29]. Only the root for γ_j that is within the first quadrant (or k_{zj} within the fourth quadrant) is selected according to the Sommerfeld radiation condition [17]. In practice, the propagation constant γ_i value in the source layer (the ith) is calculated first, then the propagation constant in all other layers can be found by

$$\gamma_j = \sqrt{k_\rho^2 - k_j^2} = \sqrt{\gamma_p^2 + \omega^2(\epsilon_p\mu_p - \epsilon_j\mu_j)} \text{ for all } j \neq p. \tag{9.8}$$

Here, all $\gamma_j's$ are functions of $\{\omega, \gamma_p\}$.

The regular local reflection coefficients at an interface between two semi-infinite media with index $i = 1..n$ for all $R_{i+}^{TE,TM}$ and $i = 0..n$ for all $R_{i-}^{TE,TM}$ are

$$R_{i\pm}^{TE} = \begin{cases} 0, & \text{with a continuous half-space} \\ -1, & \text{with a PEC ground plane} \\ \frac{\gamma_i \mu_{i\mp1} - \gamma_{i\mp1}\mu_i}{\gamma_i \mu_{i\mp1} + \gamma_{i\mp1}\mu_i}, & \text{otherwise} \end{cases}$$

and

$$R_{i\pm}^{TM} = \begin{cases} 0, & \text{with a continuous half-space} \\ 1, & \text{with a PEC ground plane} \\ \frac{\gamma_i \epsilon_{i\mp1} - \gamma_{i\mp1}\epsilon_i}{\gamma_i \epsilon_{i\mp1} + \gamma_{i\mp1}\epsilon_i}, & \text{otherwise.} \end{cases}$$

The generalized reflection coefficient along the $+\hat{z}$ direction at $z = 0$ is

$$\tilde{R}_{1+}^{TE,TM} = R_{1+}^{TE,TM}$$

then recursively for $i = 2..n$

$$\tilde{R}_{i+}^{TE,TM} = \frac{R_{i+}^{TE,TM} + \tilde{R}_{(i-1)+}^{TE,TM} e^{-2\gamma_{i-1}d_{i-1}}}{1 + R_{i+}^{TE,TM} \tilde{R}_{(i-1)+}^{TE,TM} e^{-2\gamma_{i-1}d_{i-1}}}.$$

The generalized reflection coefficient along the $-\hat{z}$ direction at $z = 0$ is

$$\tilde{R}_{n-}^{TE,TM} = R_{n-}^{TE,TM}$$

then recursively, for $i = (n-1)..0$

$$\tilde{R}_{i-}^{TE,TM} = \frac{R_{i-}^{TE,TM} + \tilde{R}_{(i+1)-}^{TE,TM} e^{-2\gamma_{i+1}d_{i+1}}}{1 + R_{i-}^{TE,TM} \tilde{R}_{(i+1)-}^{TE,TM} e^{-2\gamma_{i+1}d_{i+1}}}.$$

The local transmission coefficient at $z = 0$ is

$$S_{1+}^{TE,TM} = \begin{cases} 1 - R_{1+}^{TE,TM}, & \text{if it is used to calculate } G_x^\phi \\ 1 + R_{1+}^{TE,TM}, & \text{otherwise} \end{cases}$$

then for $q = 2..n$

$$S_{q+}^{TE,TM} = \begin{cases} \frac{1 - R_{q+}^{TE,TM}}{1 - R_{(q-1)-}^{TE,TM} \tilde{R}_{(q-1)+}^{TE,TM} e^{-2\gamma_{q-1}d_{q-1}}}, & \text{if it is used to calculate } G_x^\phi \\ \frac{1 + R_{q+}^{TE,TM}}{1 - R_{(q-1)-}^{TE,TM} \tilde{R}_{(q-1)+}^{TE,TM} e^{-2\gamma_{q-1}d_{q-1}}}, & \text{otherwise} \end{cases}$$

For every fixed field layer index p, the generalized transmission coefficients for the varying source layer index $j = (p+1)..n$ are

$$\bar{T}^{(jp)^+}_{TE,TM} = S^{TE,TM}_{j+} \prod_{q=p+1}^{j-1} e^{-\gamma_q d_q} S^{TE,TM}_{q+}.$$

The running product is unity if the upper limit is smaller than the lower limit. Additionally, the $\tilde{M}$ factors are given by

$$\tilde{M}^{TE,TM}_i = \frac{1}{1 - \tilde{R}^{TE,TM}_{i+} \tilde{R}^{TE,TM}_{i-} e^{-2\gamma_i d_i}}$$

for $i = 1..n$.

9.2.2 Green's Functions for an Arbitrary Frequency

The Green's functions for the case where both the source and field points are in the p-th layer is

$$\begin{aligned}
\tilde{G}^{\phi(pp)} \;=\; & \frac{1}{2\gamma_p\epsilon_p}\{e^{-\gamma_p|z_f - z_s|} \\
& + \frac{\omega^2\epsilon_p\mu_p}{\omega^2\epsilon_p\mu_p + \gamma_p^2}\tilde{M}^{TE}_p[\tilde{R}^{TE}_{p+}e^{-\gamma_p(2h_{p-1}-z_f-z_s)} + \tilde{R}^{TE}_{p-}e^{-\gamma_p(z_f+z_s-2h_p)} \\
& + \tilde{R}^{TE}_{p+}\tilde{R}^{TE}_{p-}(e^{-\gamma_p(2d_p+z_f-z_s)} + e^{-\gamma_p(2d_p-z_f+z_s)})] \\
& - \frac{\gamma_p^2}{\omega^2\epsilon_p\mu_p + \gamma_p^2}\tilde{M}^{TM}_p[\tilde{R}^{TM}_{p+}e^{-\gamma_p(2h_{p-1}-z_f-z_s)} + \tilde{R}^{TM}_{p-}e^{-\gamma_p(z_f+z_s-2h_p)} \\
& - \tilde{R}^{TM}_{p+}\tilde{R}^{TM}_{p-}(e^{-\gamma_p(2d_p+z_f-z_s)} + e^{-\gamma_p(2d_p-z_f+z_s)})]\}.
\end{aligned} \tag{9.9}$$

NOTE: The Green's functions used in the previous chapters do not include the factor of ϵ_p in $\tilde{G}^{\phi}$.

The Green's function take different forms for the case where the source point is in the j-th layer and the field point is in the p-th layer ($j \neq p$). By virtue of reciprocity [30] $\tilde{G}^{ij}(z_s, z_f) = \tilde{G}^{ji}(z_f, z_s)$, therefore, only the cases of $j = (p+1)..n$ need to be discussed. Assume $j > p$, $z_f > z_s$, then

$$\begin{aligned}
\tilde{G}^{\phi(pj)} \;=\; & \frac{1}{2\gamma_j\epsilon_j(\omega^2\epsilon_p\mu_p + \gamma_p^2)}\{\omega^2\epsilon_j\mu_j\bar{T}^{(jp)+}\tilde{M}^{TE}_j \\
& \cdot[e^{-\gamma_j(h_{j-1}-z_s)} + \tilde{R}^{TE}_{j-}e^{\gamma_j(z_s+h_{j-1}-2h_j)}] \\
& \cdot[e^{-\gamma_j(z_f-h_p)} + \tilde{R}^{TE}_{p+}\,e^{-\gamma_p(2h_{p-1}-h_p-z_f)}] \\
& + \gamma_j^2\bar{T}^{(jp)+}_{TM}\tilde{M}^{TM}_j \\
& \cdot[e^{-\gamma_j(h_{j-1}-z_s)} - \tilde{R}^{TM}_{j-}e^{-\gamma_j(z_s+h_{j-1}-2h_j)}] \\
& \cdot[e^{-\gamma_p(z_f-h_p)} - \tilde{R}^{TM}_{p+}\,e^{-\gamma_p(2h_{p-1}-h_p-z_f)}]\;\}.
\end{aligned} \tag{9.10}$$

9.2.3 The Static Green's Functions

Although there is little difference between the general frequency-dependent Green's functions and the static Green's functions ($\omega = 0$) procedure-wise, when the spectral Green's functions are evaluated and fitted into a series of complex exponentials before using the Sommerfeld identity for the inverse Fourier transform, the expressions of the static Green's functions are simpler. In the static case,

$$\gamma_p = \gamma \tag{9.11}$$

is independent of the index p. For the case where both the source and field points are in the p-th layer, If all layers are non-magnetic, i.e., $\mu_i = \mu_0$ for all i's, then all $\tilde{R}^{TE} = 0$, and

$$\begin{aligned}\tilde{G}^{\phi(pp)} &= \frac{1}{2\gamma\epsilon_p}\{e^{-\gamma|z_f - z_s|} \\ &\quad -\tilde{M}_p^{TM}[\tilde{R}_{p+}^{TM} e^{-\gamma(2h_{p-1}-z_f-z_s)} + \tilde{R}_{p-}^{TM} e^{-\gamma(z_f+z_s-2h_p)} \\ &\quad -\tilde{R}_{p+}^{TM}\tilde{R}_{p-}^{TM}(e^{-\gamma(2d_p+z_f-z_s)} + e^{-\gamma(2d_p-z_f+z_s)})]\}. \end{aligned} \tag{9.12}$$

The Green's function for the case where the source point is in the j-th layer and the field point is in the p-th layer ($p \neq j$) with $j = (p+1)..n$ (or $j > p$) and $z_f > z_s$ is, assuming all layers are non-magnetic,

$$\begin{aligned}\tilde{G}^{\phi(pj)} &= \frac{1}{2\gamma\epsilon_j}\bar{T}_{TM}^{(jp)+}\tilde{M}_j^{TM} \\ &\quad [e^{-\gamma(h_{j-1}-z_s)} - \tilde{R}_{j-}^{TM} e^{-\gamma(z_s+h_{j-1}-2h_j)}] \\ &\quad [e^{-\gamma(z_f-h_p)} - \tilde{R}_{p+}^{TM}\, e^{-\gamma(2h_{p-1}-h_p-z_f)}]\ . \end{aligned} \tag{9.13}$$

9.2.4 Complex Image Technique

It is possible to approximate a general spectral Green's function described above in terms of a sum of complex exponentials [18][25]

$$\tilde{G}^{\phi}(\gamma; z_s, z_f) = \frac{1}{2\gamma}\sum_{i=1}^{M}\alpha_i e^{-\gamma_j a_i} \tag{9.14}$$

where γ_j is for the source layer. The spatial domain is then determined by [13] following (9.2), or

$$G^{\phi}(x, x'; z_s, z_f) = \frac{1}{2\pi}\int_{-\infty}^{\infty} d\gamma \tilde{G}^{\phi}(\gamma; z_s, z_f) e^{j\gamma(x-x')}.$$

Use (9.14), the integral yields

$$G^{\phi}(x,x';z_s,z_f)=\frac{1}{2\pi\epsilon_s}\sum_{i=1}^{M}\alpha_i\ln\frac{1}{\sqrt{\left|\frac{x-x'}{X_0}\right|^2+\left(\frac{a_i}{X_0}\right)^2}}, \tag{9.15}$$

where

$$X_0=1 \text{ meter.}$$

The constants $a_i's$ and $\alpha_i's$ constitute the so-called complex images. The term in $G^{\phi}(x,x';z_s,z_f)$ with $a_i=0$ is identified as the "direct term" which represents a singularity when $|x-x'|=0$. Therefore, (9.15) can be written as

$$G^{\phi}(x,x';z_s,z_f)=G^{\phi}_{direct}(x,x';z_s,z_f)+G^{\phi}_{indirect}(x,x';z_s,z_f)$$

where

$$\begin{aligned}
G^{\phi}_{direct}(x,x';z_s,z_f) &= \frac{1}{2\pi\epsilon_s}\alpha_D\ln\frac{1}{\left|\frac{x-x'}{X_0}\right|},\\
G^{\phi}_{indirect}(x,x';z_s,z_f) &= \frac{1}{2\pi\epsilon_s}\sum_{i=1,a_i\neq 0}^{M}\alpha_i\ln\frac{1}{\sqrt{\left|\frac{x-x'}{X_0}\right|^2+\left(\frac{a_i}{X_0}\right)^2}}.
\end{aligned}$$

9.3 Method of Moment Formulation for Computing the C Matrix

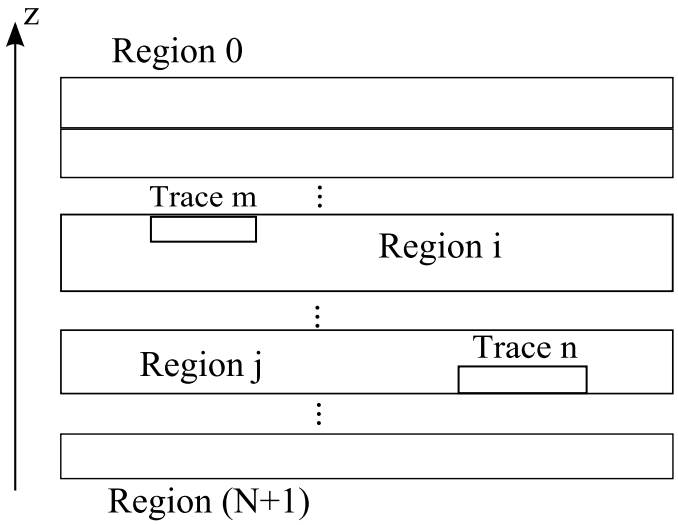

Figure 9.2: Traces in a multi-layered dielectric media.

As shown in Figure 9.2, two arbitrary traces indexed m and n are drawn. Each trace characterized by its width and thickness is modeled by a rectangular metal shell (shell has zero thickness). All edges of the rectangle of a typical trace, say Trace m, are divided into small segments, as illustrated by Figure 9.3. Line segments are the fundamental constructs that are interacting with each other.

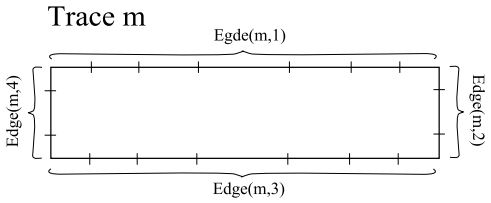

Figure 9.3: Edges of a typical trace are divided into line segments.

It is known that the charge density on a typical edge is not uniformly distributed. As a matter of fact, the charge density function takes the form of

$$\sigma(\xi) = \frac{P_0}{\sqrt{1-(2\xi/w)^2}} \tag{9.16}$$

assuming a local coordinate system shown in Figure 9.4, where P_0 is a constant. It is suggested by [31] that the edge should not be evenly divided. Instead, the center positions of the segments follow the abscissas of a Chebyshev-Gauss quadrature. Specifically, in the local coordinates (in ξ), these points are calculated by

$$\xi_k = \frac{w}{2}\cos(\frac{2k-1}{2N_\xi}\pi) \text{ for } k = 1, 2, .., N_\xi \tag{9.17}$$

with N_ξ being the number of segments along an edge.

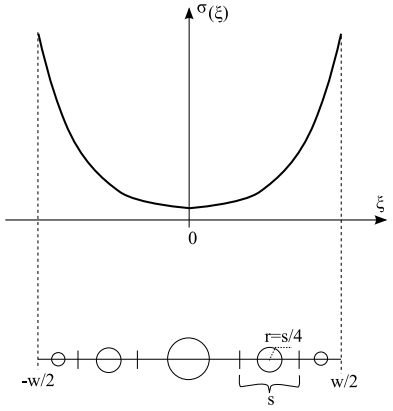

Figure 9.4: One typical edge of a trace.

The benefit of this particular way of dividing edges into segments naturally account for the charge density distribution characterized by (9.16) if each segment has the same amount of total charge.

With method of moment (MOM), all metal boundaries are divided into segments. Treating each segment as a basic unit, a system of segments are formed. The integral of (9.1) is transformed to a set of linear equations. The potential associated with Segment-m is related with the charge of at Segment-n by

$$\phi_m = K_{mn}\sigma_n \tag{9.18}$$

where the interaction terms (inverse capacitance in unit) can be computed with [31]

$$K_{mn} = \begin{cases} G^\phi_{direct}(x_m, x'_n; z_s, z_f) + G^\phi_{indirect}(x_m, x'_n; z_s, z_f) \text{ if } m \neq n \\ G^\phi_{direct}(0, r_m; z_s, z_f) + G^\phi_{indirect}(x_m, x'_n; z_s, z_f) \text{ if } m = n \end{cases}$$

where the quantity r_m is a "pipe radius" corresponding to each segment along an edge, as shown in Figure 9.4. Actually, $r'_m s$ can be immediately evaluated, once the center coordinates are calculated

with (9.17), by

$$r_m = \frac{w}{8} \frac{1}{\prod_{i=1, i \neq m} \frac{|\xi_m - \xi_i|}{w/2}},$$

noticing that the coordinates can be more efficiently stored in dimension-less form of $\xi_i/(w/2)$.

The matrix representation of (9.18) is

$$[\mathbf{\Phi}] = [\mathbf{K}][\sigma],$$

which can be inverted to have

$$[\sigma] = [\mathbf{K}]^{-1}[\mathbf{\Phi}].$$

Denote

$$\mathbf{C}_{seg} = [\mathbf{K}]^{-1} \tag{9.19}$$

which is the segment level capacitance matrix. Suppose that there are M traces, due to the fact that each trace has the same potential for all its constituent segments. The raw capacitance matrix of (9.19) can be reduced to a $M \times M$ matrix $\mathbf{C}$ using the following algorithm:

for each segment i
{
    determine trace index $m(i)$;
    for each segment j
    {
        determine trace index $n(j)$;
        $C_{mn} += C_{raw}(i, j)$;
    }
}

It is assumed that the $\mathbf{C}$ matrix elements were initially set to zeros. The $m(i)$ and $n(j)$ are the mapping from the segment index to the trace index.

Bibliography

[1] C. R. Paul, *Analysis of Multiconductor Transmission Lines*. Wiley Interscience, 1994.

[2] E. Recht and S. Shiran, "A simple model for characteristic impedance of wide microstrip lines for flexible pcb," in *EMC Symposium*, pp. 1010–1014., 2000.

[3] T. K. S. Antonije R. Djordjevic, Miodrag B. Bazdar and R. F. Harrington, *LINPAR Manual*. Artech House, 1990.

[4] J. D. G. Swanson and W. J. R. Hoefer, *Microwave Circuit Modeling using Electromagnetic Field Simulation*. Artech House, 2003.

[5] L. A. H. Dylan F. Williams and R. B. Marks, "A complete multimode equivalent-circuit theory for electrical design," *J. Res. Natl. Inst. Stand. Technol.*, vol. 102, pp. 405–423, 1997.

[6] F. O. E. L. Luc F. Knockaert, Daniël De Zutter and J. D. Geest, "Recovering lossy multiconductor transmission line parameters from impedance or scattering representations," *IEEE Transactions on Advanced Packaging*, vol. 25, pp. 200–205, May 2002.

[7] B. Young, *Digital Signal Integrity*. New Jersey: Prentice Hall, 2011.

[8] J. W. L. M. H. Wu, W. J. Chen and X. B. Fang, "An improvement method of the increasing mutual capacitance for reducing far-end crosstalk in transmission line," in *IEEE Antennas and Propagation Society International Symposium*, pp. 1227 – 1230, 2006.

[9] W. Shi and J. Fang, "Evaluation of closed-form crosstalk models of coupled transmission lines," *IEEE Transactions on Advanced Packaging*, vol. 22, pp. 174–181, May 1999.

[10] J. R. M. Wei Cao, R. F. Harrington and T. K. Sarkar, "Multiconductor transmission lines in multilayered dielectric media," *IEEE Transactions on Microwave Theory and Techniques*, vol. 32, pp. 439–450, April 1984.

[11] R. F. H. J. R. Mautz and C. G. Hsu, "The inductance matrix of a multiconductor transmission line in multiple magnetic media," *IEEE Transactions on Microwave Theory and Techniques*, vol. 36, pp. 1293–1295, August 1988.

[12] H. A. Wheeler, "Skin resistance of a transmission-line conductor of polygon cross section," *Proceedings of the IRE*, vol. 43, pp. 805–808, July 1955.

[13] F. M. J. Bernal and M. Horno, "Quick quasi-tem analysis of multiconductor transmission lines with rectangular cross section," *IEEE Transactions on Microwave Theory and Techniques*, vol. 45, pp. 1619–1626, September 1997.

[14] T. Kitazawa and R. Mittra, "Analysis of asymptotic coupled striplines," *IEEE Transactions on Microwave Theory and Techniques*, vol. 33, pp. 643–646, 1985.

[15] W. J. Getsinger, "Dispersion of parrallel-coupled microstrip," *IEEE Transactions on Microwave Theory and Techniques*, vol. 21, pp. 144–145, 1973.

[16] K. J. Scott, "Efficient image theory for electromagnetic field modelling in pcb," *Phillips Journal of Research*, vol. 48, no. 1-2, pp. 37–61, 1994.

[17] W. C. Chew, *Waves and Fields in Inhomogeneous Media*. IEEE Press, New Jersey, 1995.

[18] D. G. F. Y. L. Chow, J. J. Yang and G. E. Howard, "A closed-form spatical green's function for the thick microstrip substrate," *IEEE Transactions on Microwave Theory and Techniques*, vol. 39, no. 3, pp. 588–592, 1991.

[19] R. M. Shubair and Y. L. Chow, "Efficient computation of periodic green's function in layered dielectric media," *IEEE Transactions on Microwave Theory and Techniques*, vol. 41, pp. 498–502, March 1993.

[20] G. Dural and M. I. Aksun, "Closed-form green's functions for general sources and stratified media," *IEEE Transactions on Microwave Theory and Techniques*, vol. 43, pp. 1545–1552, July 1995.

[21] M. I. Askun and G. Dural, "Closed-form green's functions of hed, hmd, ved and vmd for multilayer media," in *Proceedings of IEEE Antennas and Propagations Society International Symposium*, (Ann Arbor, MI, USA), pp. 354–357, June 1993.

[22] M. I. Askun, "A robust approach for the derivation of closed-form green's functions," *IEEE Transactions on Microwave Theory and Techniques*, vol. 44, pp. 651–658, May 1996.

[23] K. M. Lale Alatan, M. I. Aksun and M. T. Birand, "Analytical evaluation of the mom matrix elements," *IEEE Transactions on Microwave Theory and Techniques*, vol. 44, pp. 519–525, April 1996.

[24] N. Kinaman and M. I. Askun, "Efficient use of closed-form green's functions for the analysis of planar geometries with vertical connections," *IEEE Transactions on Microwave Theory and Techniques*, vol. 45, pp. 593–603, May 1997.

[25] Y. Hua and T. K. Sarkar, "Generalized pencil-of-function method for extracting poles of an em system from its transient response," *IEEE Transactions on Antennas and Propagation*, vol. 37, pp. 229–234, February 1989.

[26] T. K. Sarkar and O. Pereira, "Using the matrix pencil method to estimate the parameters of a sum of complex exponentials," *IEEE Antennas and Propagation Magazine*, vol. 37, pp. 48–55, February 1995.

[27] O. F. Ming-Ju Tsai, Franco De Flaviis and N. G. Alexopoulos, "Modeling planar arbitrary shaped microstrip elements in multilayered media," *IEEE Transactions on Microwave Theory and Techniques*, vol. 45, pp. 330–337, March 1997.

[28] D. M. Pozar, *Microwave Engineering*. New York: Addison Wesley, 1990.

[29] J. W. Brown and R. V. Churchill, *Complex Variable and Applications*. New York: McGraw-Hill, 1996.

[30] C. A. Balanis, *Advanced Engineering Electromagnetics*. New York: John Wiley, 1989.

[31] J. J. Y. Gregory E. Howard and Y. L. Chow, "A multipipe model of general strip transmission lines for rapid convergence of integral equation singularities," *IEEE Transactions on Microwave Theory and Techniques*, vol. 40, no. 4, pp. 628–636, 1992.